nature communications

Article

https://doi.org/10.1038/s41467-024-51918-1

Proximity interactome of lymphatic VE-cadherin reveals mechanisms of junctional remodeling and reelin secretion

Received: 30 March 2023

Accepted: 20 August 2024

Published online: 04 September 2024

Check for updates

D. Stephen Serafin[1,2], Natalie R. Harris[1,2], László Bálint[1], Elizabeth S. Douglas[1] & Kathleen M. Caron[1]

The adhesion receptor vascular endothelial (VE)-cadherin transduces an array of signals that modulate crucial lymphatic cell behaviors including permeability and cytoskeletal remodeling. Consequently, VE-cadherin must interact with a multitude of intracellular proteins to exert these functions. Yet, the full protein interactome of VE-cadherin in endothelial cells remains a mystery. Here, we use proximity proteomics to illuminate how the VE-cadherin interactome changes during junctional reorganization from dis-continuous to continuous junctions, triggered by the lymphangiogenic factor adrenomedullin. These analyses identified interactors that reveal roles for ADP ribosylation factor 6 (ARF6) and the exocyst complex in VE-cadherin trafficking and recycling. We also identify a requisite role for VE-cadherin in the in vitro and in vivo control of secretion of reelin—a lymphangiocrine glycoprotein with recently appreciated roles in governing heart development and injury repair. This VE-cadherin protein interactome shines light on mechanisms that control adherens junction remodeling and secretion from lymphatic endothelial cells.

VE-cadherin (gene = *Cdh5*) is a central adherent component of endothelial adherens junctions (AJs) and serves as critical mediator of endothelial cell permeability and vascular integrity[1,2]. The blood vasculature holds an absolute requirement for VE-cadherin during development to maintain closed circulation of blood and prevent vascular leakage. The requirement for VE-cadherin in the lymphatic vasculature has recently been demonstrated using a lymphatic specific genetic knockout mouse[3,4]. Developmental loss of VE-cadherin results in edema and embryonic lethality due to the inability of naïve lymphatic vessels to remodel into a functional vasculature[3] as well as form functional lymphatic valves[4]. Post-natal loss of VE-cadherin leads to progressive and severe structural deterioration of intestinal lacteals[3], mesenteric lymphatics[3,4] and cardiac lymphatics[5] while other vessel beds, like dermal lymphatics, were anatomically preserved but dysfunctional. This highlights a critical role for VE-cadherin in the blood and lymphatic vasculatures.

VE-cadherin localizes to the plasma membrane of endothelial cells to form AJ complexes which participate in the transduction of a large variety of extracellular signals regulating cell growth, cell polarity, lumen formation, and responses to fluid shear stress[6–10]. This is achieved through trans-homophilic interactions between VE-cadherin extracellular domains, association with plasma membrane proteins and receptors at its transmembrane domain, and through coordinated interaction with a wide variety of intracellular molecules at its C-terminal tail including molecules like catenins, plakoglobin, and p120[9,11]. Spatial arrangement of VE-cadherin at endothelial cell contacts is directly linked to vessel permeability and region-specific vessel function. In blood vessels and collecting lymphatics, VE-cadherin is positioned in a continuous fashion, creating low permeability vessels capable of shuttling blood or lymph to various parts of the body. In lymphatic capillaries, VE-cadherin is sparsely patterned at cell borders in a discontinuous fashion, creating overlapping junction-free zones

[1]Department of Cell Biology and Physiology, University of North Carolina at Chapel Hill, 111 Mason Farm Road, Chapel Hill 27599 NC, USA. [2]These authors contributed equally: D. Stephen Serafin, Natalie R. Harris. e-mail: kathleen_caron@med.unc.edu

that allow for facile uptake of interstitial fluid and large molecules like lymphocytes and pathogens into lymphatic circulation[6,12]. VE-cadherin junctional conformations in capillary lymphatics are highly plastic and are readily converted from one arrangement to another upon stimulation by inflammatory molecules, lymphangiogenic peptides, developmental cues, and disease[6,9,13–15]. For example, the lymphangiogenic peptide, adrenomedullin (AM), rapidly alters lymphatic VE-cadherin AJs from an open, dis-continuous arrangement to a closed, continuous junction[13,16]. Taken together, this necessitates the existence of a diverse network of interactions to hold VE-cadherin in different junctional conformations and to enable VE-cadherin to exert its numerous cellular functions.

Proximity proteomics have emerged as a powerful tool to identify the composition of proteins which come into close vicinity of a protein of interest in a living cell. Proximity-dependent biotin identification (BioID)[17] relies on the fusion of a promiscuous biotin ligase to a bait protein to enable promiscuous biotin tagging of lysine residues of proximal proteins within a narrow radius of the fusion protein. These biotinylated proteins are then enriched by a streptavidin affinity-purification (AP) and profiled by western blot analysis and/or mass spectrometry. The resultant protein interactome captures both direct protein interactions as well as weak, indirect, transient, and spatial interactions often not detected by conventional methods of protein-protein interaction discovery. The BioID method has been applied with great success to five different junctional proteins including ZO-1[18], E-cadherin[19,20], N-cadherin[21], occludin and claudin-4[22] and has provided significant insight into the cadherin interactome and organization of epithelial cellular junctions.

BioID technology has rapidly evolved with numerous new generations of BioID ligases recently developed[17,23]. These new generation BioID enzymes, TurboID and miniTurboID, offer improved catalytic activity which can efficiently biotinylate proximal proteins in as little as 15 min as compared to the 16–24 h needed for comparable biotinylation by earlier generations of BioID ligases[24]. Therefore, the technology is ideal for the capture of highly temporal and transient interactions, such as those occurring during rapid cell barrier tightening and reorganization of VE-cadherin AJs induced by AM signaling[13,16].

In this work, we utilize (Mini)TurboID-based proximity proteomics to profile how the VE-cadherin proximal protein interactome in lymphatic endothelial cells (LECs) changes in response to AM stimulation. Using a suite of bioinformatic analyses, we identify conserved classical cadherin interactors and probe pathways mediating VE-cadherin trafficking and AJ remodeling through mechanistic inhibitor studies and identify a novel connection between VE-cadherin, AM, and the lymphangiocrine molecule reelin.

Results

VE-cadherin-miniTurbo responds to AM-junctional remodeling

To meet the physiologic demands across the lymphatic plexus, VE-cadherin is arranged in two unique conformations, a permeable dis-continuous junction and largely impermeable continuous junction[25,26]. VE-cadherin AJs undergo rapid reorganization when stimulated by barrier disrupting or tightening agents, indicating the need for highly coordinated protein interactions. AM is a lymphangiogenic peptide hormone which potently reorganizes and stabilizes the lymphatic endothelial barrier both in vivo and in vitro by modulating VE-cadherin AJs[13]. Thus, we sought to define the VE-cadherin proximal protein interactome during AM-mediated junctional rearrangement using BioID proteomics (Fig. 1A, B).

We cloned VE-cadherin into a ubiquitin C-driven lentiviral expression vector system containing C- terminal V5-tagged TurboID or V5-tagged miniTurboID. Cellular expression of these constructs yields a VE-cadherin-V5-TurboID (VE-cad-T or VE-cadherin-T) or VE-cadherin-V5-miniTurboID (VE-cad-mT or VE-cadherin-mT) fusion protein which biotinylates proteins within an approximate radius of 10 nm[17,24,27]. VE-cadherin-T and VE-cadherin-mT constructs were transiently transfected into biotin-supplemented HEK293Ts to validate fusion-protein expression, protein biotinylation efficiency, and localization (Supplementary Fig. 1A). We saw robust expression of both VE-cadherin fusion-proteins when blotting for the incorporated V5-epitope. Streptavidin blotting revealed a robust time-dependent increase in biotinylated proteins for both VE-cadherin-T and VE-cadherin-mT. However, significant background biotinylation was noted in the VE-cadherin-T expressing cells that did not receive exogenous biotin relative to VE-cadherin-mT expressing cells in line with previously published reports[24,28]. This background biotinylation was even more pronounced in HEK293Ts stably expressing VE-cadherin-T and VE-cadherin-mT fusion-proteins (Supplementary Fig. 1B). This lack of temporal control with the VE-cadherin-T construct guided our decision to use the VE-cadherin-mT construct for subsequent LC-MS/MS experiments.

Using confocal microscopy, we found that VE-cadherin-mT fusion protein localized as expected along cell-cell junctions in transiently transfected HEK293Ts (Supplementary Fig. 1C). Biotinylation capacity of the cells was confirmed using streptavidin-AlexaFluor 488. With the addition of biotin, we observed VE-cadherin-mT-expressing cells displaying diffuse and weak streptavidin staining within the cytosol and robust staining at cell-cell junctions in near complete overlap with VE-cadherin expression. Streptavidin affinity-purification (AP) of biotinylated proteins from VE-cadherin-mT-lentivirus transduced HEK293T whole-cell lysates revealed a time-dependent enrichment of biotinylated proteins, successful pulldown of VE-cadherin-mT, as shown by blotting for V5, and ß-catenin, a known VE-cadherin-interactor (Supplementary Fig. 1D). Confocal microscopy corroborated these results showing a time-dependent increase in VE-cadherin-proximal protein biotinylation over an hour of biotin treatment, as seen by increasing streptavidin-AlexaFluor 488 signal at cell-cell junctions (Supplementary Fig. 1E).

Having satisfactorily confirmed VE-cadherin-mT function in HEK293Ts, we evaluated fusion protein expression, function, and localization in LECs (Fig. 1C, D). These primary LECs, obtained from pooled male donors, provide an ideal system to study AM-induced VE-cadherin junctional remodeling due to their expression of endogenous VE-cadherin and regulatory machinery. Streptavidin AP was performed on whole cell lysates from LECs transduced with VE-cadherin-mT lentivirus and treated with 50 μM biotin for 2 h, which resulted in enrichment of biotinylated proteins and capture of VE-cad-mT fusion protein and β-catenin. Co-treatment with 100 nM AM resulted in a modest increase in VE-cadherin-mT fusion protein and ß-catenin, suggesting an increased recruitment of these proteins upon AM stimulation (Fig. 1C). Next, we investigated whether the VE-cadherin-mT fusion protein is capable of forming and rearranging AJs. Confocal microscopy of LECs confirmed that both native VE-cadherin and VE-cadherin-mT fusion-protein rearrange into predominately continuous junctions upon AM treatment. Additionally, we found protein biotinylation was strongest along cell-cell junctions, indicated by Streptavadin-AlexaFluor 488 (Fig. 1D). Together, this data indicates VE-cadherin-mT can capture the VE-cadherin interactome during AM-induced AJ rearrangement in LECs.

Profiling of the global lymphatic VE-cadherin interactome

To identify the VE-cadherin proximal protein interactome during AM-mediated junctional rearrangement, we performed LC-MS/MS mass spectrometry on streptavidin AP proteins obtained from the whole cell lysates of VE-cadherin-mT expressing LECs treated with 100 nM AM or vehicle and labeled with 50 μM biotin for 2 h (Fig. 1B). Analysis of two independent experiments on whole cell lysates (Supplementary Data 1 and 2) allowed us to investigate the global intracellular interactome of VE-cadherin, which encompasses

https://doi.org/10.1038/s41467-024-51918-1

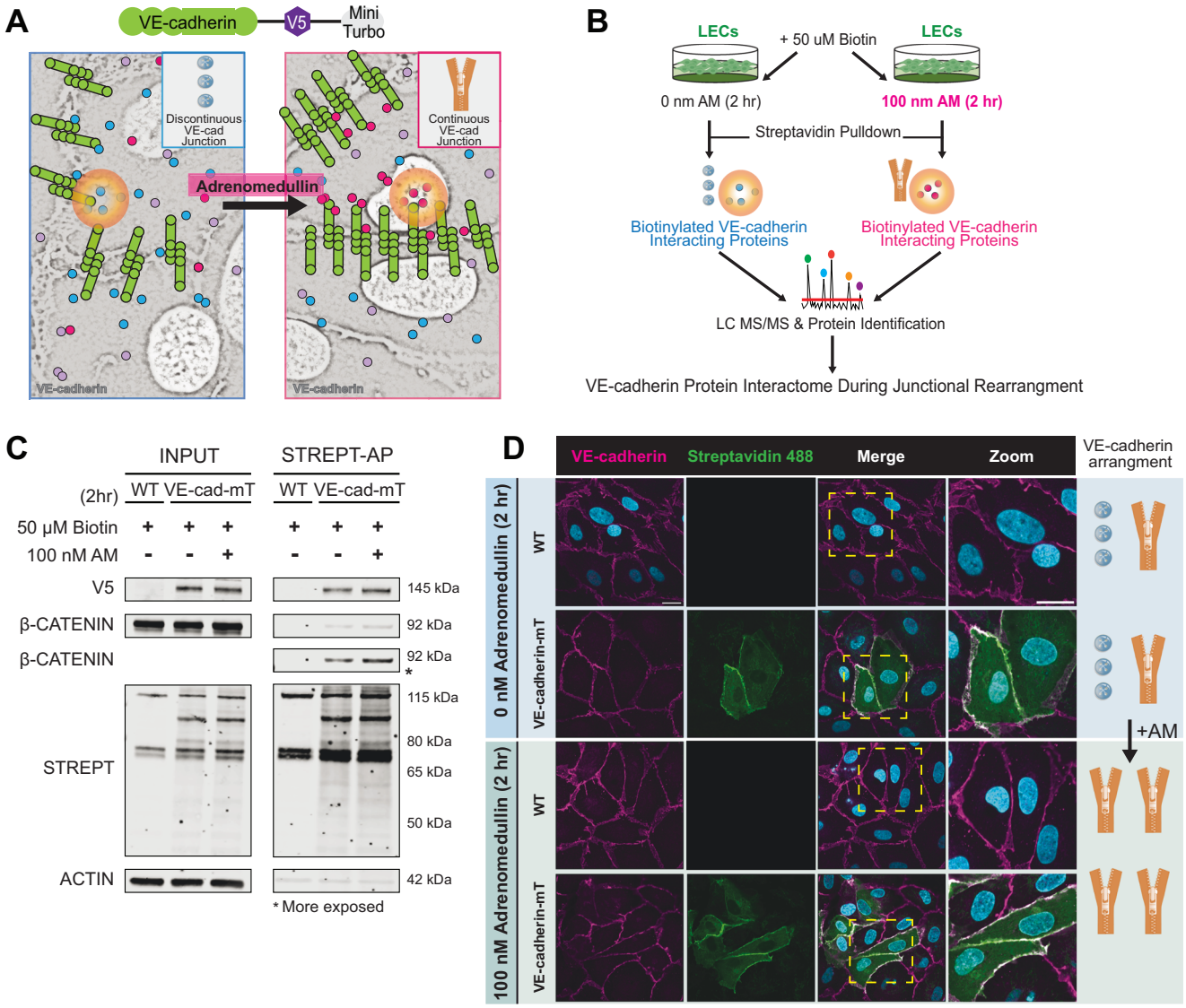

Fig. 1 | Validation of a functional VE-cadherin-V5-miniTurbo that recapitulates native VE-cadherin AM-induced junctional rearrangement in LECs. A Schematic of adrenomedullin (AM)-mediated rearrangement of VE-cadherin; a central component on inter-endothelial adherens junctions. AM induces the rapid rearrangement of discontinuous junctions to continuous VE-cadherin junctions. **B** Experimental workflow used to obtain the VE-cadherin interactome during junctional rearrangements (predominantly discontinuous with 0 nM AM; predominantly continuous with 100 nM AM). **C** LECs were transduced with VE-cadherin-V5-miniTurbo (VE-cad-mT) lentivirus and treated with vehicle or 100 nM AM and 50 μM biotin for a 2 h labeling period to evaluate fusion protein expression and biotinylation by western blot after streptavidin affinity-purification. Anti-V5 evaluated fusion protein expression, streptavidin probed biotinylated proteins, ß-catenin probed a known VE-cadherin-interactor, and actin served as a load control. Shown is a representative experiment. A minimum of three independent experiments were performed. **D** Confocal microscopy to evaluate the cellular localization of VE-cadherin-mT fusion protein in transduced primary LECs treated with vehicle or 100 nM AM and 50 μM biotin for a 2 h labeling period. Cells were stained for VE-cadherin (magenta) to detect VE-cadherin-mT fusion proteins as well as native VE-cadherin, streptavidin (green) to stain for biotinylated proteins, and DAPI (cyan) to mark cell nuclei. Scale bar = 20 μm. A minimum of three independent experiments were performed. Source data are provided with this paper.

pathways involved in trafficking and localization to the plasma membrane.

The promiscuous nature of the miniTurboID biotin ligase results in background biotinylation of proteins related to transcription and translation of bait-miniTurboID fusion proteins and biologically irrelevant transient proximity to structures, including mitochondria, ribosomes, and the nucleus. Additionally, the miniTurboID workflow often captures viral infection associated proteins due to transduction of cells with bait-miniTurboID lentivirus as well as biotinylation due to native biotin carboxylases. Therefore, we manually curated the protein list of VE-cadherin interacting proteins to remove these contaminants, similar to other cadherin-interactome reports[19–21] (Fig. 2, Supplementary Data 1). Specifically, we removed proteins with Gene Ontology (GO) terms associated with ribosomes, RNA, translation, mitochondria, nuclear localization, RNA splicing, transcription, viral infection, DNA binding, keratin contaminants, and biotin carboxylases (Supplementary Data 1). This manual curation was performed to remove proteins which were biotinylated independent of the VE-cadherin-miniTurbo construct or bound non-specifically to the streptavidin-coated beads. A limitation of this approach is that true interactors (type II error; false negatives) or non-specific interactors (type I error; false positive) may have been erroneously excluded or included. As such, we provide the full un-curated dataset within Supplementary Data 1 and 2.

Next, we performed GO pathway analysis[29–31] on the manually curated list of 763 VE-cadherin interacting proteins to identify the

https://doi.org/10.1038/s41467-024-51918-1

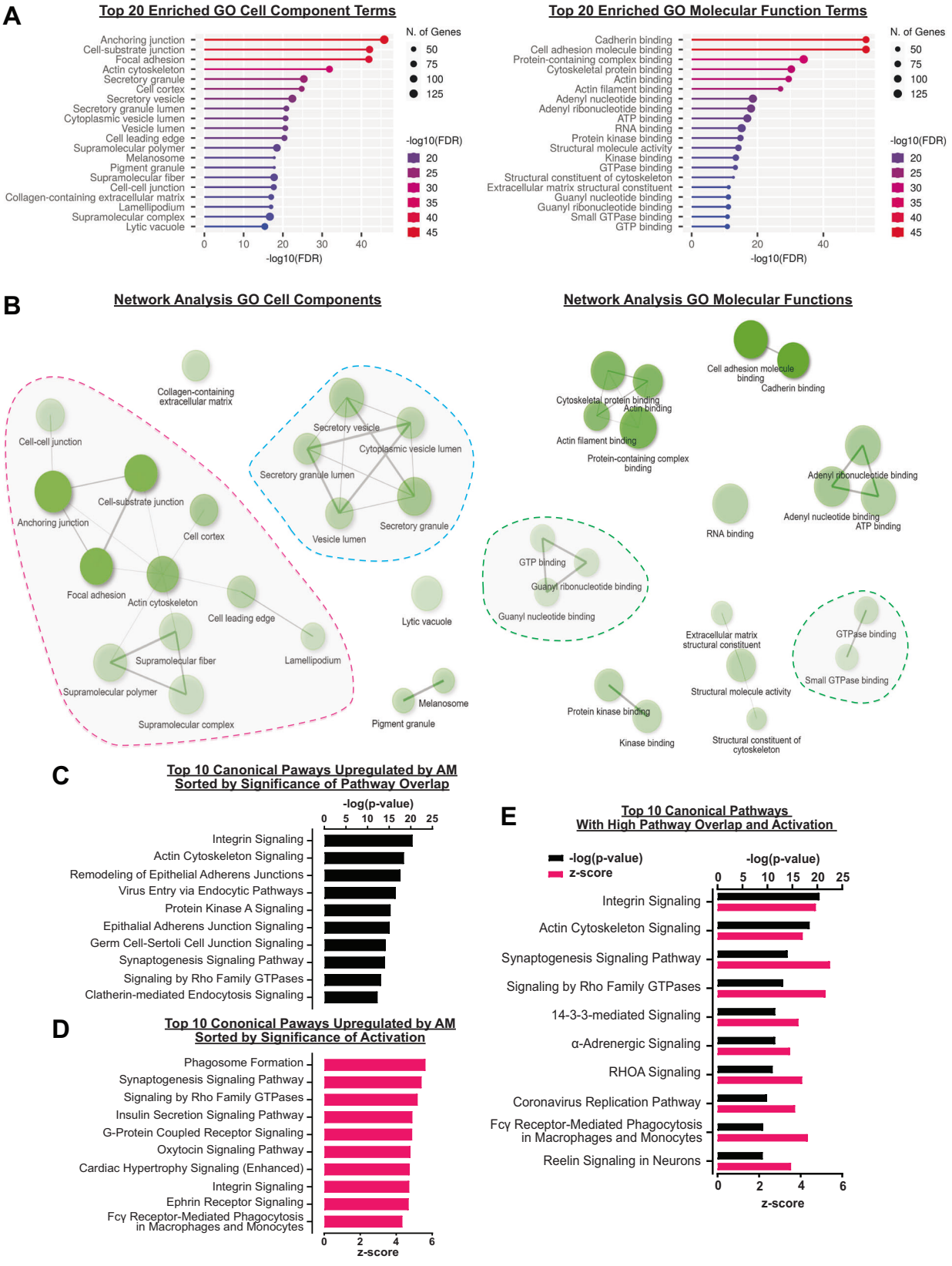

cellular and molecular functions of the VE-cadherin interactors (Fig. 2). As expected, anchoring junctions, cell-substrate junctions, and focal adhesions were the top 3 enriched cell component GO terms (Fig. 2A, Supplementary Data 3), indicating VE-cadherin-mT possesses a high degree of specificity for labeling proteins proximal to AJs. Cell components associated with vesicles and large molecule complexes were also readily identified (i.e. secretory granules and vesicles). This was visualized through network analysis, which revealed two large discrete super nodes relating to cell adhesion/actin organization (pink outline; 11 interconnected nodes) and vesicular structures (blue outline; 5 interconnected nodes) (Fig. 2B). When examining the top 20 most enriched GO Molecular Functions, we found cadherin binding

Fig. 2 | Bioinformatic analysis of the AM-induced VE-cadherin interactome identifies enrichment of secretory and Rho family GTPase pathways. A Gene Ontology (GO) Cell Component and Molecular Function annotation of top 20 most significant terms determined by enrichment false discovery rate (FDR), which indicates how likely the enrichment of the term is by chance and where smaller values correlate with a lower likelihood of random enrichment. Bar length correlates to enrichment FDR (displayed as -log10(FDR)) and the size of bar-terminating circles correlates to the number of genes found within that term. **B** Network analysis of top 20 enriched GO Cell Components and GO Molecular Functions annotations showing relationship between pathways. Node size correlates to size of gene sets, intensity and opacity of green shading refers to enrichment of gene sets (light/transparent indicates lower degree of enrichment, dark/opaque indicates higher degree of enrichment). Two pathways are considered connected if gene overlap between sets is >20% and is denoted by lines between nodes. Thickness of lines correlates to the degree of gene overlap between nodes. Pink outline indicates the 'cell adhesion/actin organization super-node'.Blue outline indicates the 'vesicular structures super-node'. Green outline indicates the 'GTPase super-nodes'. **C** Top 10 enriched canonical pathways identified by Ingenuity Pathway Analysis (IPA) sorted by significance of number of proteins overlapping with the pathway (pathway overlap). Values displayed are -log(*p*-value) calculated by IPA (right-tailed Fisher's exact test). **D** Top 10 enriched canonical pathways identified by IPA sorted by significance of activation of the pathway. Values displayed are z-scores calculated by IPA. **E** Top 10 Pathways with both high pathway overlap and activation. Both -log(*p*-value) and *z*-score are plotted for each pathway (right-tailed Fisher's exact test). Source data are provided with this paper.

and cell adhesion molecule binding to be the most enriched, followed by cytoskeletal and actin regulation functions (Fig. 2A, Supplementary Data 3). Molecular function analysis also revealed significant enrichment of GTP and ATP activities, both of which are well known for regulating vesicular transport[32] and factors affecting VE-cadherin adhesiveness[11]. In fact, network analysis of the top 20 enriched GO Molecular Functions revealed super-clusters related to GTP binding and GTPase activity (Fig. 2B).

We next layered in the effect of AM-induced junctional rearrangement by performing Ingenuity Pathway Analysis (IPA) on the proteins in the whole cell VE-cadherin interactome after AM treatment (Supplementary Data 4). We examined AM-upregulated canonical pathways by (1) the number of interactors overlapping with a pathway (Fig. 2C) and (2) the predicted pathway activation (Fig. 2D). In accordance with GO analysis, we found a high degree of VE-cadherin interactome overlap (-log(*p*-value)) with integrin signaling, actin cytoskeleton signaling, and remodeling of epithelial AJs (Fig. 2C). We found a slightly different set of pathways to be significantly activated (z-score), including phagosome formation, synaptogenesis signaling, and signaling by RHO family GTPases (Fig. 2D). When integrating significance of pathway overlap and pathway activation (Fig. 2E), we encountered expected enrichment of certain canonical pathways (i.e. integrin signaling, actin cytoskeleton signaling, and Rho signaling) and rather unexpected enrichment of pathways not typically associated with endothelial cells (i.e. reelin signaling in neurons).

Comparative analysis of the classical cadherin interactomes

In recent years, BioID proximity proteomics have been employed to capture the interactome of two Type I classical cadherins, E-cadherin and N-cadherin[19–21], which revealed an intriguing set of conserved and distinct classical cadherin interactors. We sought to further expand the classical cadherin interactome by performing a three-way analysis between the E-cadherin, N-cadherin, and VE-cadherin interactomes. This analysis draws comparisons between Type I and Type II classical cadherins, species and tissue-specific interactions, and proximity labeling dynamics of different generations of BioID ligases (Supplementary Fig. 2A). The cadherin interactomes, specifically Uniprot associated protein names, were obtained from Guo et al., (E-cadherin)[19], Li et al., (N-cadherin)[21], and from the whole cell lysate VE-cadherin interactome (Supplementary Data 1). The protein names were used as input values for quantitative comparison and proportional visualization of list overlap using BioVenn software[33] (Supplementary Fig. 2B, Supplementary Data 5). A total of 38 proteins were found to be conserved across all three cadherins. Using 20 pre-determined functional categories derived from information from Uniprot and established by Li et al., [21], the 38 conserved interactors were assigned cellular functions (Supplementary Fig. 2C). Adapters (actin binding adapters, membrane binding adapters, and adapters) were the largest category represented at a combined 45%. Represented among the 38 conserved interactors are known cadherin interactors related to junctional integrity, including α-Catenin, ß-Catenin, δ-Catenin, Junction Plakoglobin, and Talin-1 (Supplementary Fig. 2D). Additionally, proteins central to structures expected to be proximal to AJs were also found, such as tight junction protein ZO-2. Interestingly, proteins typically only associated with a single cadherin, such as Emerin, which only is known to associate with E-cadherin and AJs between intercalated disks[34], were found to associate with all three cadherins from different cell types. Next, we matched all 38 conserved interactors to their log2 fold change when VE-cadherin-mT LECs were treated with AM to induce cell junction rearrangement (Supplementary Fig. 2D). A substantial proportion of these proteins, 33 out of 38, were found to be significantly enriched (Log2 fold change > 1) by AM treatment, indicating a dynamic response of the VE-cadherin interactome. Together, this data demonstrates the utility of BioID proximity proteomics to delineate classical cadherin interactomes and has identified a set of conserved interactors sensitive to stimuli influencing junctional arrangements.

Profiling of the lymphatic membrane VE-cadherin interactome

To investigate membrane-specific changes in the VE-cadherin interactome, we performed LC-MS/MS on streptavidin AP proteins obtained from isolated plasma membrane (PM) fractions of VE-cadherin-mT expressing LECs treated with 100 nM AM or vehicle and labeled with 50 μM biotin for 2 h (Supplementary Data 6). Streptavidin AP confirmed the presence of the VE-cad-mT fusion protein within isolated membrane fractions and resulted in modest enrichment of biotinylated interactors (Fig. 3A). Similar to the current whole cell VE-cadherin interactome, we used Gene Ontology (GO) terms to remove contaminants from the PM-derived VE-cadherin interactome. The full un-curated dataset is provided in Supplementary Data 6. Next, we compared the list of proteins identified in the whole cell- and PM-derived VE-cadherin interactomes (Fig. 3B). The total number of PM identified proteins was expectedly and significantly smaller (254 total) than proteins identified in the whole cell lysate (763 total). Importantly, we found that 60.2% of PM identified interactors were shared with the whole cell samples, indicating that plasma membrane isolation identifies a unique subset of proteins found in the global VE-cadherin interactome. Next, we explored enriched biological pathways in the PM-derived VE-cadherin interactome using Reactome pathway analysis[35] (Fig. 3C, Supplementary Data 7). Strong pathway overlap was noted for multiple clusters including vesicle-mediated transport, signal transduction, and cell-cell communication. Closer examination of the cell-cell communication cluster showed strong overlap with the adherens junctions interactions pathway (Fig. 3D), which consisted of known VE-cadherin and AJ interactors including catenins, actin, and afadin (Fig. 3E). We validated Reactome identification of afadin (Supplementary Fig. 3A) and β-catenin (Supplementary Fig. 3B) within LECs transduced with VE-cadherin-mT. Taken together, these analyses demonstrate the reproducibility and specificity of VE-cadherin-mT fusion protein to biotinylate VE-cadherin- and AJ-proximal protein interactors.

https://doi.org/10.1038/s41467-024-51918-1

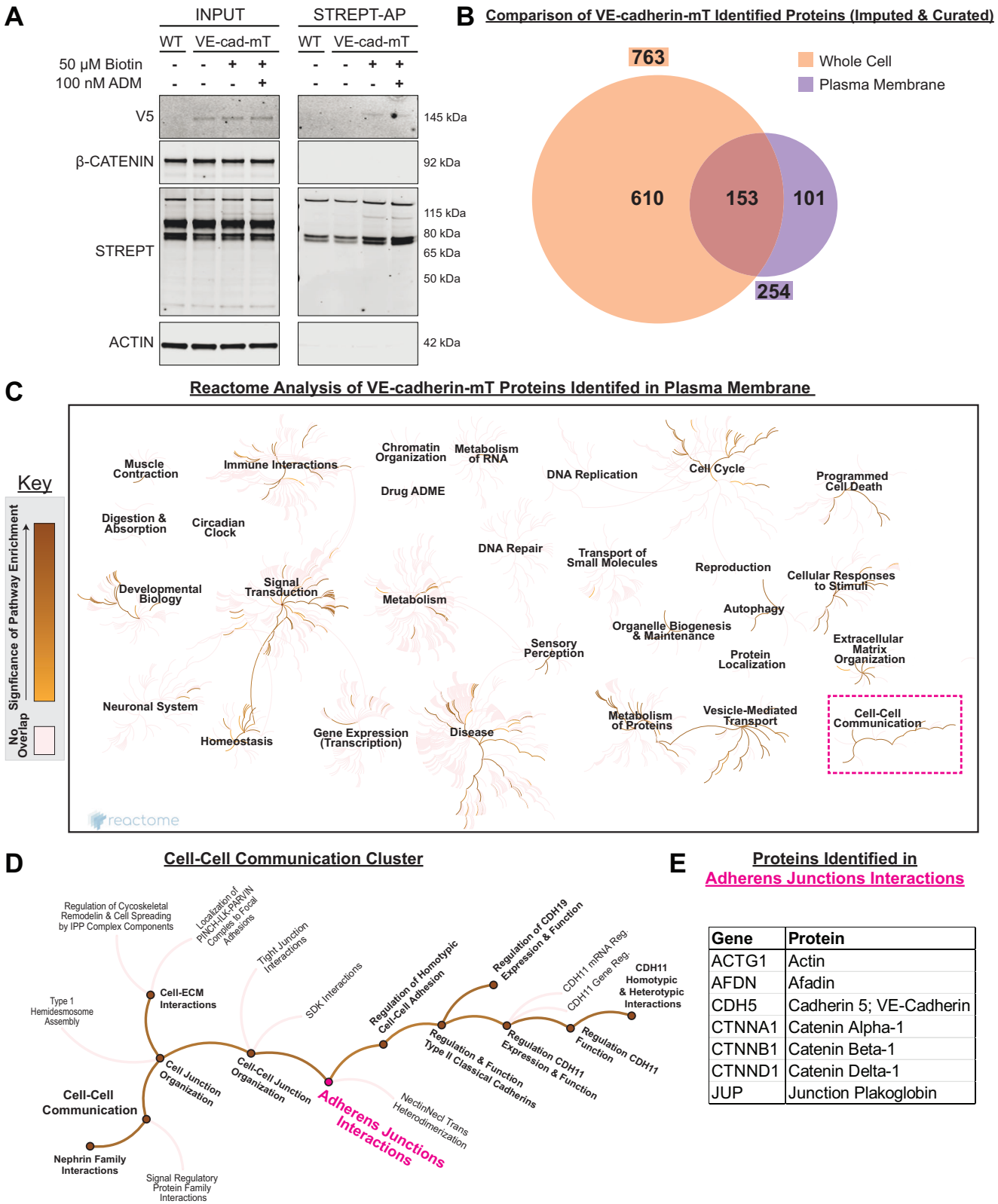

Gene	Protein
ACTG1	Actin
AFDN	Afadin
CDH5	Cadherin 5; VE-Cadherin
CTNNA1	Catenin Alpha-1
CTNNB1	Catenin Beta-1
CTNND1	Catenin Delta-1
JUP	Junction Plakoglobin

We performed GO pathway analysis on the PM-derived VE-cadherin interactome (Fig. 4). Examination of the top 20 enriched GO cell components and molecular function terms identified strong signals associated with vesicles and large molecule complexes (i.e. secretory granules and vesicles), focal adhesion and junctional proteins, as well as GDP/GTP activation (Fig. 4A). These signals are prominent in the network analysis, which shows three large discrete super nodes for focal adhesions (outlined in pink), vesicles and secretory granules (outlined in blue), and GDP/GTP activation (outlined in green) (Fig. 4B). Further, examination of the top 20 enriched GO biological processes revealed a large signal for active secretion and exocytosis (Supplementary Fig. 4A, B).

Next, we performed Ingenuity Pathway Analysis (IPA) on proteins that showed enrichment of Log2 > 0.5 for 'biotin' versus 'no biotin'

Fig. 3 | Comparative analysis of VE-cadherin interactomes identified in whole cell or plasma membrane fractions reveals reproducibly captured proteins and pathways. A Detection of VE-cad-mT, ß-catenin, and biotinylated protein isolated from LEC plasma membrane cell fractions. Membrane isolation was performed on LECs that were transduced with VE-cad-mT and treated with vehicle or 100 nM AM and 50 μM biotin for a 2 h labeling period, followed by streptavidin affinity purification and western blot analysis. INPUT and STREPT-AP fractions were profiled for V5 to evaluate fusion protein expression and pulldown, streptavidin to probe biotinylated proteins, ß-catenin to probe for a known VE-cadherin-interactor, and actin served as a load control. Shown is a representative experiment. A minimum of three independent experiments were performed. **B** Venn diagram of proteins uniquely or repeatedly captured across VE-cadherin interactomes generated from whole cell lysate (WCL1) or plasma membrane (PM) fractions. **C** Reactome[35] analysis of proteins identified in the PM VE-cadherin interactome. Within clusters, branches and nodes with increasing orange color refers to increased significance of overlap with individual pathways comprising a cluster. Pink dashed box refers to (**D**). **D** Zoomed in view of the Cell-Cell Communication cluster showing expected enrichment of pathways associated with junction organization and adherens junctions. **E** List of proteins, with their gene names, identified in the PM VE-cadherin interactome which are sorted to the 'Adherens Junction Interactions' node of the Reactome Cell-Cell Communication Cluster. Source data are provided with this paper.

(Fig. 4C), 'biotin and AM' versus 'no biotin' (Fig. 4D), and 'biotin and AM' versus 'biotin' (Fig. 4E). Shown are the top 20 pathways with high pathway overlap (-log(*p*-value)) and activation (z-score) for each comparison. Compared to a no biotin control, we found a high degree of VE-cadherin interactome overlap and activation with sertoli cell-germ cell signaling, epithelial adherens junction signaling and remodeling, and cell-junction organization (Fig. 4C, D). Further, when comparing 'biotin + AM' versus 'biotin only', we found a high degree of VE-cadherin interactome overlap and activation with extracellular matrix organization, degradation of extracellular matrix, and integrin cell surface interactions and signaling (Fig. 4E). Interestingly, for all comparisons, we found a high degree of VE-cadherin interactome overlap and activation of synaptogenesis signaling (Fig. 4C–E), suggesting another link to reelin signaling, which was identified in whole cell-derived VE-cadherin interactome as having both high pathway overlap and activation. Taken together, the analysis of the PM-derived AM-induced VE-cadherin interactome identifies a role for secretory vesicles and GTPase activity in the remodeling of endothelial AJs.

Endo/Exocyst pathways mediate VE-cadherin junctions

When viewing this data in aggregate, we observed that AM stimulation upregulates signals for GTPase activation, junctional organization, intracellular trafficking, and secretion. Close examination of the IPA canonical pathways for remodeling of epithelial AJs and CDC42 signaling showed a conserved enrichment of numerous proteins involved in the coordinated process of cadherin internalization, endosomal sorting, and recycling to the plasma membrane (PM), leading us to generate a model of VE-cadherin AJ remodeling (Fig. 5A). Specifically, the whole cell VE-cadherin interactome showed strong AM-mediated enrichment of ARF6, dynamin (DNM), Rab5, 6 of 8 components of the exocyst complex, and CDC42BPA. We sought to investigate the importance of these interactors in lymphatic VE-cadherin AJ remodeling by profiling VE-cadherin and β-catenin membrane levels in LECs using pharmacological and genetic approaches (Fig. 5B–D).

We first assessed whether ARF6-DNM mediated endocytosis and recycling, a process shown to be critical for E-cadherin trafficking[36], affected PM levels of VE-cadherin and ß-catenin. We treated LECs with Rasarfin, a dual Ras and ARF6 inhibitor, which significantly decreased VE-cadherin PM levels after 4 h of treatment and nearly ablated VE-cadherin levels after 24 h (Fig. 5B). In alignment with loss of VE-cadherin at the PM, we observed a significant decrease in ß-catenin PM levels at 4- and 24 h. In fact, transducing LECs with shRNA lentivirus against VE-cadherin (*Cdh5*) (referred to as shCDH5) not only resulted in an expected significant decrease in VE-cadherin mRNA transcript levels (Supplementary Fig. 5A, B) and total protein expression but further resulted in a similar significant decrease in total β-catenin protein expression (Supplementary Fig. 6A).

The EX complex is a large 8 subunit and Ral GTP-ase regulated[37] complex that has been widely demonstrated in epithelial cells to regulate guided exocytosis of E-cadherin-containing recycling endosomes to the plasma membrane, resulting in region specific redistribution of surface E-cadherin[38]. We found that 6 of 8 of the EX-complex subunits were strongly enriched in the whole cell VE-cadherin interactome (Supplementary Data 1, Fig. 5A). Therefore, we sought to explore the effect of EX-complex inhibition on VE-cadherin PM levels. First, we treated cells with Endosidin-2, a chemical exocyst-complex inhibitor, and assessed relative PM levels of VE-cadherin and ß-catenin (Fig. 5C). Endosidin-2 treatment produced a modest decrease in VE-cadherin PM levels at 4 h, which became significant after 24 h of treatment. ß-catenin PM levels were slightly reduced at 4 h but decreased significantly by 24 h, in alignment with VE-cadherin.

Amongst the 6 EX-complex subunits enriched in the VE-cadherin interactome, EXOC5 (Sec10) displayed the strongest enrichment with AM treatment (5.04 log2(fold change)). We found this enrichment to be particularly exciting, as EXOC5 has been identified as a downstream effector of active ARF6-GTP and helps mediate delivery of recycling membranes to select areas of the PM undergoing reorganization[39]. Thus, we sought to specifically inhibit the EXOC5 subunit of the EX-complex by transducing LECs with shRNA against EXOC5 (shEXOC5) and study the resultant effect on VE-cadherin PM levels. The knockdown efficiency of shEXOC5 clones was validated by qPCR (Supplementary Fig. 7A) and protein expression (Supplementary Fig. 7B). We transduced LECs with shScramble control lentivirus or shEXOC5-967 (now referred to as shEXOC5) lentivirus for 48 h and subsequently treated the cells with AM or vehicle for 4 or 24 h (Fig. 5D). VE-cadherin PM levels were significantly decreased in shEXOC5 transduced LECs relative to shScramble LECs. Interestingly, unlike Rasarfin or Endosidin-2 treatments, there was no change in ß-catenin PM levels in shEXOC5 transduced LECs.

To determine if membrane loss of VE-cadherin and β-catenin in LECs was the result of decreased VE-cadherin transcription or enhanced degradation, we performed western blot analysis on total protein levels of both VE-cadherin and β-catenin as well as qPCR of VE-cadherin (*Cdh5*) mRNA post-treatment with Rasarfin, Endosidin2, or shEXOC5. Rasarfin treatment of LECs did not significantly affect VE-cadherin mRNA production nor total VE-cadherin protein levels at 4 h or β-catenin protein levels at 4- or 24 h post-treatment. Rasarfin significantly decreased total VE-cadherin protein levels 24 h post-treatment (Supplementary Fig. 5C & D, Supplementary Fig. 6B). Endosidin2 did not significantly change VE-cadherin mRNA or total protein at 4 h post-treatment but resulted in significant decreases in both VE-cadherin mRNA and total VE-cadherin and β-catenin protein at 24 h post-treatment (Supplementary Fig. 5E, F, Supplementary Fig. 6C). Surprisingly, shEXOC5 significantly increased VE-cadherin mRNA transcript levels (Supplementary Fig. 5G, H) but had no effect on total VE-cadherin or β-catenin protein levels (Supplementary Fig. 6D). In all cases, AM treatment did not affect either VE-cadherin transcription or VE-cadherin or β-catenin protein levels (Fig. 5, Supplementary Fig. 5, Supplementary Fig. 6). Taken together, these data suggest that observed decreases in VE-cadherin PM levels are largely the result of enhanced VE-cadherin degradation upon inhibition of VE-cadherin endocytic-exocyst recycling mechanisms.

https://doi.org/10.1038/s41467-024-51918-1

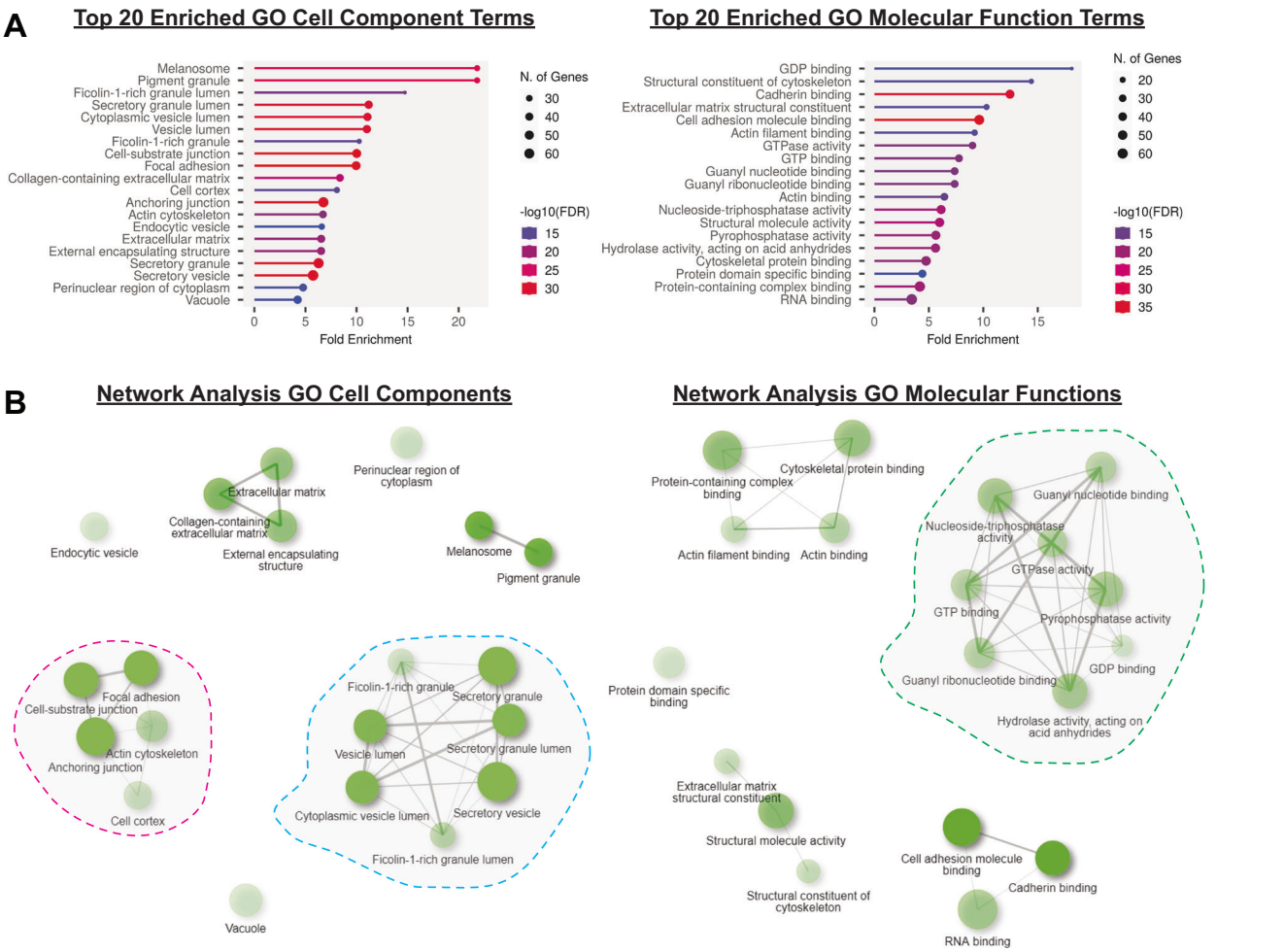

Inhibition of endo/exocyst pathways disrupt VE-cadherin

To visualize the effect of disrupting VE-cadherin AJs remodeling, we examined VE-cadherin localization at LEC cell-cell junctions using confocal microscopy (Fig. 6A) and quantified the effect of AM on cell-cell junction morphology (Fig. 6B). Controls (DMSO for Rasarfin and Endosidin-2 or shScramble for shEXOC5) showed the typical pattern of VE-cadherin staining at cell-cell junctions and response to AM by increasing the proportion of continuous junctions. Rasarfin produced a profound effect on VE-cadherin localization, resulting in puncta-like islands of VE-cadherin surrounded by areas completely devoid of VE-cadherin. AM co-treatment had no effect. In complete opposite, Endosidin-2 produced near complete and continuous staining of

Fig. 4 | Bioinformatic analysis of the plasma membrane-specific AM-induced VE-cadherin interactome identifies a role for secretory vesicles and GTPase activity in the remodeling of epithelial adherens junctions. A Gene Ontology (GO) Cell Component and Molecular Function annotation of top 20 most significant terms determined by enrichment false discovery rate (FDR), which indicates how likely the enrichment of the term is by chance and where smaller values correlate with a lower likelihood of random enrichment. Bar length correlates to enrichment FDR (displayed as -log10(FDR)) and the size of bar-terminating circles correlates to the number of genes found within that term. **B** Network analysis of top 20 enriched GO Cell Components and GO Molecular Functions annotations showing relationship between pathways. Node size correlates to size of gene sets, intensity and opacity of green shading refers to enrichment of gene sets (light/transparent indicates lower degree of enrichment, dark/opaque indicates higher degree of enrichment). Two pathways are considered connected if gene overlap between sets is >20% and is denoted by lines between nodes. Thickness of lines correlates to the degree of gene overlap between nodes. Pink outline indicates the 'cell adhesion/actin organization super-node'. Blue outline indicates the 'vesicular structures super-node'. Green outline indicates the 'GTPase super-node'. **C**–**E** Top 20 Pathways with high pathway overlap (significance of proteins overlapping with the pathway; displayed as -log(*p*-value)) and activation (displayed as *z*-score) when comparing samples that received (**C**) biotin versus a no biotin control, (**D**) biotin + AM versus a no biotin control, and (**E**) biotin + AM versus biotin only. Both -log(*p*-value) (right-tailed Fisher's exact test) and z-score are plotted for each pathway. IPA analysis included all proteins having a log2 value > 0.5. $n = 3$ biological replicates of 'biotin' and 'biotin + AM'. Source data are provided with this paper.

VE-cadherin at cell-cell borders, which similar to Rasarfin, was not affected by AM treatment. The most striking effect on VE-cadherin localization was observed in shEXOC5 transduced LECs, which displayed profuse and elongated VE-cadherin projections extending between cells, akin to patterns of junctional deformation induced by cyclic stretch[40]. Treatment with AM appeared to slightly recover these pronounced junctional deformations, as some linear staining between cells was occasionally observed. Phase contrast images of LECs treated with Rasarfin, Endosidin2, or shEXOC5 show that LECs maintain a monolayer of cells with intact cell-cell junctions (Supplementary Fig. 8). These data support that disruption of VE-cadherin trafficking and recycling impacts VE-cadherin AJ remodeling and ability to respond to AM treatment.

Lymphatic secretion of reelin requires membrane VE-cadherin

Bioinformatic analysis of the whole cell and PM-derived VE-cadherin interactomes revealed prominent signals for secretory vesicles/granules as well as active cellular export and secretion (Fig. 2, Fig. 4, Supplementary Fig. 4). Interestingly, we consistently identified the secreted glycoprotein, reelin, as significantly enriched in the VE-cadherin interactomes, which was not found in either the E- or N-cadherin interactomes. Reelin is broadly known for its role in neuronal development and migration[41], but has newly appreciated roles in lymphatic biology, such as in the recruitment of smooth muscle cells to developing lymphatic collectors[42] and as a lymphangiocrine factor that promotes cardiomyocyte proliferation during cardiac growth and repair[43]. Reelin protein was significantly enriched by AM in the whole cell VE-cadherin interactome (2.54 log2(fold change)), and the functional pathway "Reelin Signaling in Neurons" was amongst the top 10 IPA-identified canonical pathways with a high degree of pathway overlap and activation after AM treatment (Fig. 2G). Therefore, we sought to explore the connection between reelin, AM, and VE-cadherin by measuring reelin levels in conditioned media from vehicle or AM-stimulated LECs using a colorimetric reelin enzyme-linked immunosorbent assay (ELISA). In parallel, we also assessed relative VE-cadherin PM levels. In all conditions tested, there was a significant increase in reelin secretion over time (Supplementary Fig. 9). First, we probed the connection between AM and reelin section. AM-treatment resulted in a modest, yet significant, increase in reelin levels compared to vehicle, accompanied by increased levels of PM-derived VE-cadherin (Fig. 7A). These effects of AM on reelin secretion and VE-cadherin protein levels were intermittently recapitulated in other experiments (Fig. 7B–E and Supplementary Fig. 10). To examine the role of VE-cadherin on reelin secretion dynamics, we measured reelin levels in the conditioned media from LECs transduced with shScramble or shCDH5 lentivirus and treated with AM (Fig. 7B). Excitingly, knockdown of VE-cadherin produced a significant and profound reduction (>80% at 24 h) in reelin secretion overtime relative to control, which correlated with a dramatic decrease in VE-cadherin PM levels (Fig. 7B).

To probe how inhibition of VE-cadherin AJ remodeling mediates reelin secretion (Fig. 5), we assessed reelin levels in LECs treated with Rasarfin, Endosidin-2 or transduced with shEXOC5 (Fig. 7C–E). First, we tested the effect of ARF6 inhibition on reelin secretion using Rasarfin. Similar to knockdown of VE-cadherin, Rasarfin resulted in a significant reduction in reelin secretion (>75% at 24 h) relative to DMSO control (Fig. 7C). The magnitude of this reduction increased over-time and correlated with a temporal reduction in VE-cadherin PM levels (Fig. 7C). Next, we tested the effect on reelin secretion of EX-complex inhibition in LECs using Endosidin-2 (Fig. 7D) and shEXOC5 (Fig. 7E). After 24 h, reelin levels were not significantly reduced after DMSO or Endosidin-2 treatment; however, co-treatment of Endosidin-2 with AM resulted in a significant reduction in reelin levels relative to AM-treated control (Fig. 7D). Analogous to the mild impact on reelin secretion, we found that PM levels of VE-cadherin were not remarkably altered by Endosidin-2 treatment (Fig. 7D). On the other hand, knockdown of EXOC5 significantly reduced reelin secretion relative to control and correlated with reduced VE-cadherin PM levels (Fig. 7E). This data suggests that VE-cadherin AJ remodeling is critical for reelin secretion in vitro.

Given the marked impact on reelin secretion in vitro, we sought to determine whether lymphatic VE-cadherin might influence reelin secretion in vivo. To accomplish this goal, we utilized an inducible, genetic mouse model of lymphatic-specific VE-cadherin deletion (*Cdh5*$^{fl/fl}$; *Prox1*^{CreERT2}; shortened to *Cdh5*$^{\Delta ProxI}$)[3]. We tested serum reelin levels collected from adult 1–2 month-old *Cdh5*$^{\Delta ProxI}$ mice at baseline and 22 days after VE-cadherin deletion was induced by intraperitoneal injection of tamoxifen. Consistent with the in vitro data, there was a significant reduction in serum reelin levels in *Cdh5*$^{\Delta ProxI}$ mice compared to tamoxifen-injected WT controls (Fig. 7F). This data supports a newly identified role of VE-cadherin in mediating secretion of lymphangiocrine signals.

Discussion

BioID has previously been used to map the interactome of the two mammalian Type I cadherins, E-cadherin and N-cadherin. Here, we successfully used miniTurboID proximity proteomics to define how the lymphatic VE-cadherin interactome is altered in response to AM signaling (Fig. 1). Importantly, this is the first interactome of a mammalian Type II cadherin and the first BioID-based interactome in LECs. Comparative analysis between the E-cadherin, N-cadherin, and VE-cadherin interactomes identified a small, conserved list of proteins shared across the classical cadherin family and highlighted over 630 VE-cadherin-specific proximity interactions (Supplementary Data 1). This high number is likely due to the unique function of VE-cadherin in vascular endothelial cells but may also reflect differences in the catalytic efficiency of miniTurbo over earlier generations of BioID technology used to generate the E-cadherin and N-cadherin interactomes, as well as in differences in protein composition and expression across the different cell types profiled. A strength and limitation of the proximity labeling technique is that it captures relative changes in proteins within proximity of the bait, which may not necessarily reflect a change in protein abundance or expression within the cells.

https://doi.org/10.1038/s41467-024-51918-1

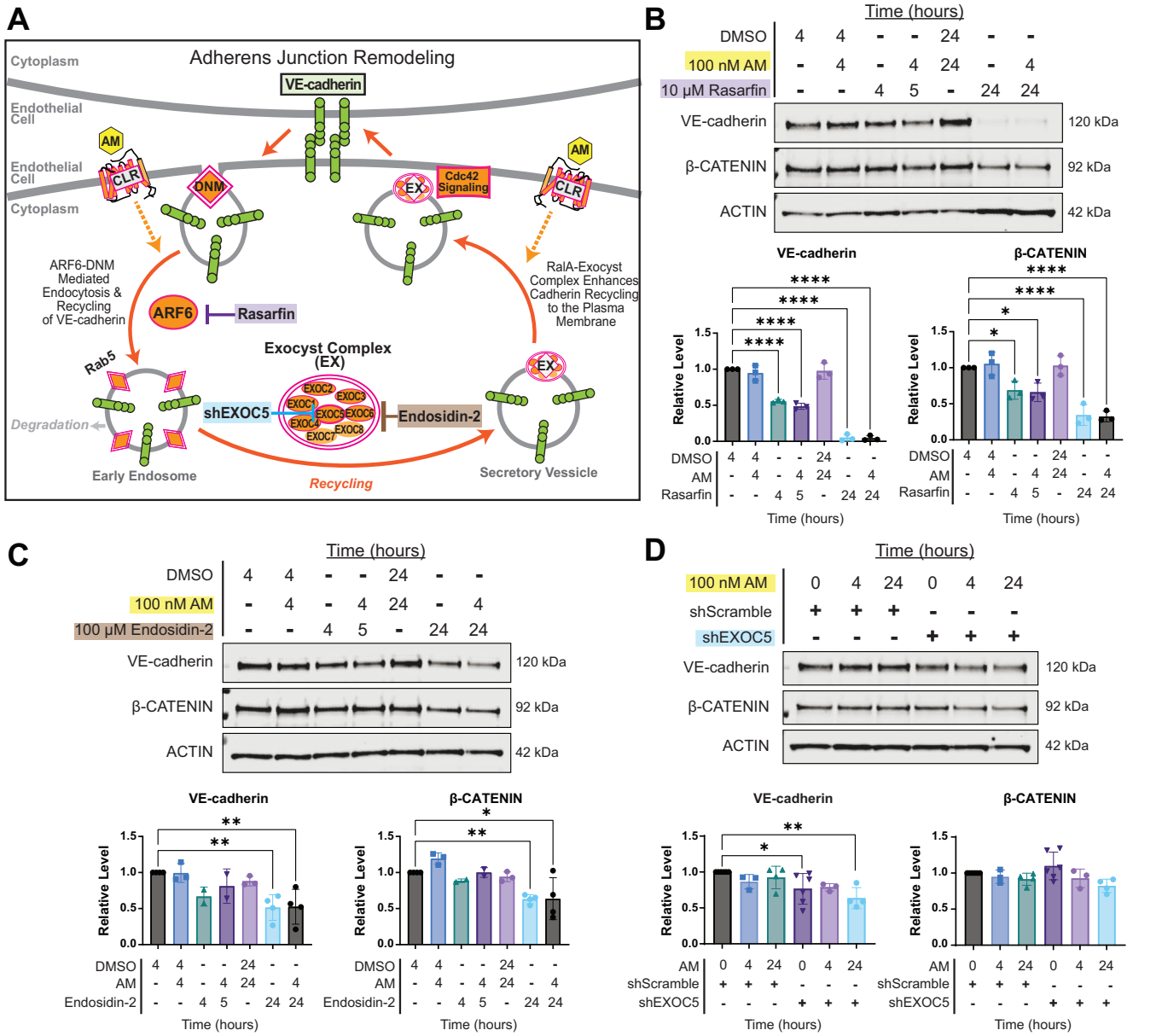

Fig. 5 | AM-mediated VE-cadherin junction remodeling occurs through an endocytic-exocyst pathway. A Proposed model of AM-mediated adherens junction regulation, generated by aggregating elements from the WCL1 highly enriched pathways "Remodeling of Epithelial Adherens Junctions" and "CDC42 Signaling". In accordance with IPA legend, pink outlines refer to proteins identified in the VE-cadherin interactome, orange fill refers to high confidence of predicted activation, orange lines with arrow heads refer to predicted activated relationships. Lines with flat heads refer to inhibition (purple refers to Rasarfin inhibition of ARF6, blue refers to shEXOC5 knockdown of EXOC5, brown refers to Endosidin-2 inhibition of Exocyst Complex (EX)). Western blot and densitometric analysis of plasma membrane fractions of LECs treated with +/− 100 nM AM as well as (**B**) 10 μM Rasarfin, (**C**) 100 μM Endosidin-2, or (**D**) shEXOC5 to determine AM, inhibitor, or shRNA time-dependent (4 or 24 h) changes on membrane-specific VE-cadherin and ß-catenin protein levels. Shown are representative blots. Densitometric quantification of VE-cadherin and ß-catenin levels were first normalized to their respective load control (actin or GAPDH) and then normalized relative control (DMSO or shScramble). Data represents $n = 3$-6 biological replicates for each inhibitor or shRNA (mean ± s.d). One-way ANOVA with Dunnett's multiple comparisons test was used to calculate significance. Precise n numbers and *p*-values are found for each condition in Supplementary Data 10. Source data are provided with this paper. $^{*}p < 0.05$, $^{**}p < 0.01$, $^{***}p < 0.001$, $^{****}p < 0.0001$.

In defining the lymphatic VE-cadherin interactome, we found that over 53% of the identified proteins were enriched by a log2(fold change) > 3.0 after AM treatment (Supplementary Data 1), demonstrating the sweeping and dynamic change to the VE-cadherin interactome during junctional rearrangement. Further, IPA and GO analyses detected significant enrichment of pathways linked to GTPase activity, vesicular trafficking, exocytosis, and secretion[11,44] (Figs. 2 and 4). To this end, we found significant enrichment of molecular machinery known to regulate the endocytosis and recycling of E-cadherin, including the GTP binding protein, ARF6, and the GTP-regulated exocyst (EX) complex.

ARF6 is known to contribute to the endocytosis and trafficking of membrane components into early endosomes as well as interacts with the EX-complex to target secretory vesicles for insertion into the plasma membrane[45]. Further, six subunits of the EX complex were identified in the WCL VE-cadherin interactome, including EXOC5 (Sec10), which was the most enriched of the EX-complex subunits after AM treatment. Interactions between GTP-bound

https://doi.org/10.1038/s41467-024-51918-1

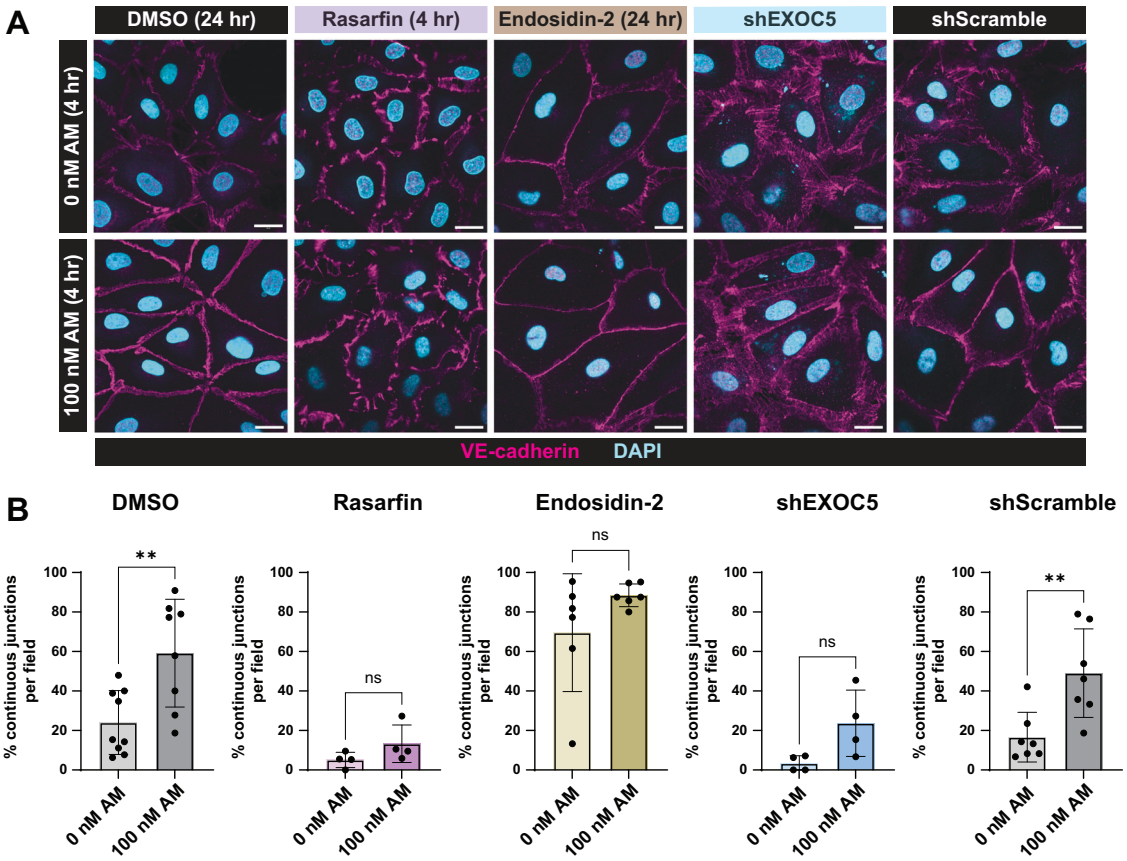

Fig. 6 | Inhibition of endocytic-exocyst pathways disrupts VE-cadherin junctional architecture in LECs. A Representative images of VE-cadherin localization in LECs co-treated with vehicle or 100 nM AM for 4 h under the following additional conditions: DMSO (24 h), 10 μM Rasarfin (4 h), 100 μM Endosidin-2 (24 h), or transduction with shScramble, or shEXOC5 lentivirus (72 h). Cells were stained for VE-cadherin (magenta) and DAPI (cyan) to mark cell nuclei. Scale bar = 20 μm. **B** Quantification of the percentage of continuous junctions per field relative to total number of junctions for each condition shown in (**A**). $n = 4$ to 9 images analyzed for each condition. Unpaired two-tailed t-tests were used to calculate significance. Precise n numbers and p-values are found for each condition in Supplementary Data 10. Source data are provided with this paper. $^{*}p < 0.05$, $^{**}p < 0.01$, $^{***}p < 0.001$, $^{****}p < 0.0001$.

ARF6 and EXOC5 are highly transient and are not readily identified by co-immunoprecipitation of endogenous proteins. In fact, this interaction was only successfully identified by co-immunoprecipitation of recombinant tagged EXOC5 and native GTP-ARF6[39]. Of note, the VE-cadherin interactome revealed robust enrichment of these proteins despite their transient interactions. Through mechanistic inhibitor studies (Figs. 5, 6), we show that both ARF6 and the exocyst complex influence membrane VE-cadherin AJ remodeling.

Recently, the glycoprotein reelin was identified as a lymphangiocrine factor capable of directly influencing heart size through regulation of cardiomyocyte proliferation[43]. Specifically, global and lymphatic-specific deletion of reelin in vivo resulted in reduced cardiomyocyte proliferation through integrinß1 signaling pathways and ectopic delivery of reelin promoted cardiac repair after infarction by dampening levels of cardiomyocyte apoptosis. Intriguingly, we consistently identified the glycoprotein reelin within both the WCL and PM VE-cadherin proximity interactomes. In future studies, it would be interesting to determine whether this is a direct VE-cadherin-interaction or a proximity of reelin to VE-cadherin AJs. Regardless, we find that reelin secretion from lymphatics is highly sensitive to VE-cadherin membrane levels within lymphatic cells in vitro and in vivo (Fig. 7B–F). This data highlights a novel link between reelin secretion and VE-cadherin, likely due to the role of VE-cadherin in mediating AJ stability. Further, we find that disruption of VE-cadherin trafficking and recycling similarly inhibits reelin secretion (Fig. 7C–E); however, these phenotypes may be, at least in part, due to disruption of shared trafficking pathways between VE-cadherin and reelin. Future work will focus on elucidating the distinct or overlapping mechanisms of reelin and VE-cadherin trafficking.

In addition to the identified link between VE-cadherin and reelin, this study further illuminated a previously unrecognized link between AM and lymphatic secretion of reelin (Fig. 7A), which likely has pathophysiological significance in the context of heart development and injury repair. This is because AM and its prohormone mid-regional pro-AM (MR-proAM) are well-established clinical biomarkers of cardiac disease[46,47] and AM has been extensively studied for its role as a potent vasodilator[48] and involvement in cardiovascular pathologies such as myocardial infarction, heart failure, preeclampsia, and sepsis[49–52]. Like reelin, genetic overexpression or exogenous application of AM leads to increased lymphangiogenesis, reduced cardiac remodeling, and improved cardiovascular function[53]. Moreover, and similar to reelin, a well-documented role of AM signaling is its ability to dose-dependently govern heart size. For example, global genetic loss of AM, or it's signaling receptor complex, calcitonin receptor like receptor (*Calcrl*; CLR) or receptor activity modifying protein 2 (*Ramp2*; RAMP2), results in smaller hearts with reduced myocyte proliferation[54,55]. Conversely, genetic overexpression of AM, or global loss of the AM decoy receptor, ACKR3/CXCR7 (*Cxcr7*$^{-/-}$) results in cardiomyocyte hyperproliferation and enlarged hearts[56,57]. Therefore, these convergent relationships raise the interesting possibility that reelin is a downstream effector of AM signaling, as both molecules have been independently linked as drivers of heart size and cardiac repair after injury. Future studies exploring this AM-VE-cadherin-reelin axis could establish whether reelin is a biomarker of

https://doi.org/10.1038/s41467-024-51918-1

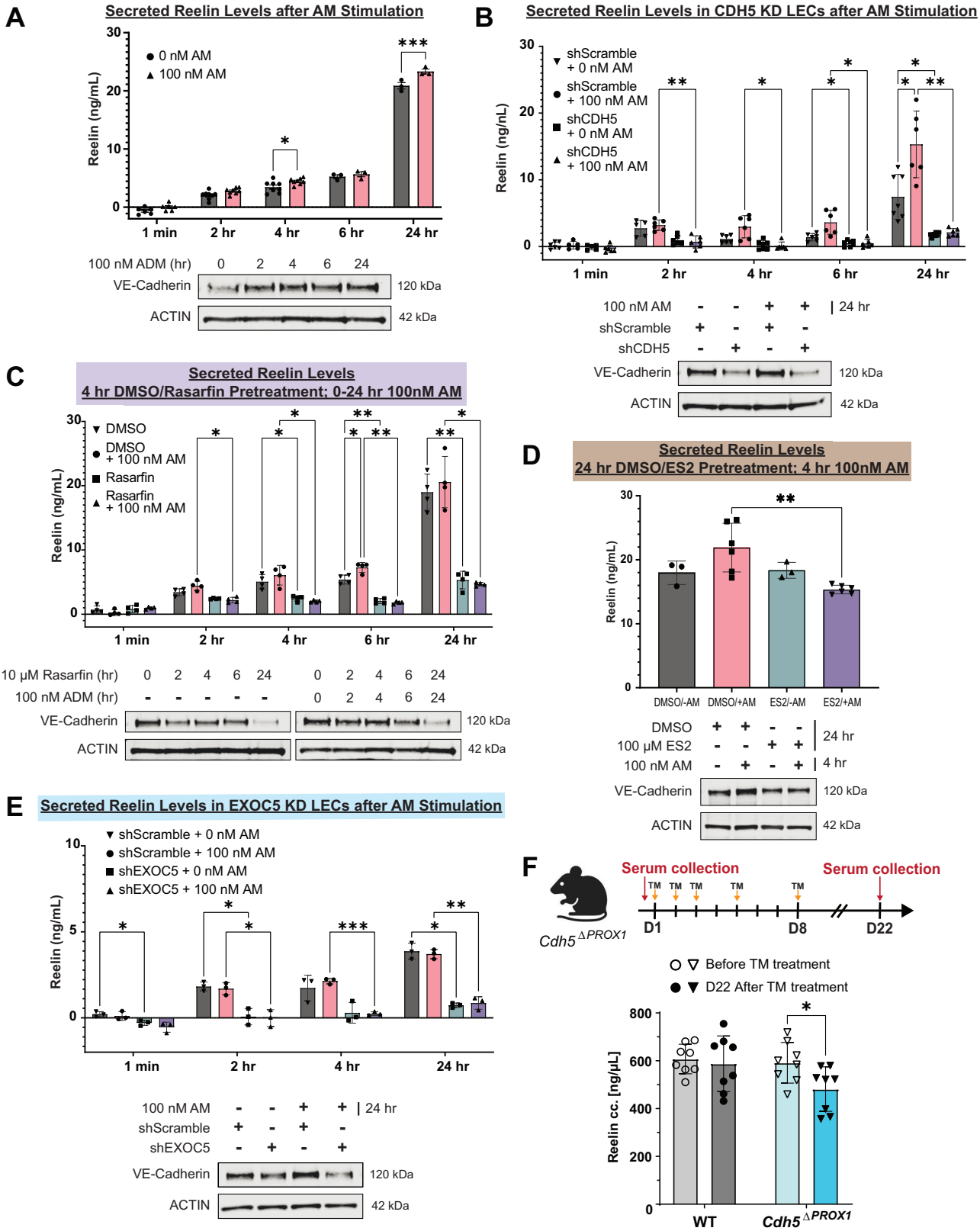

cardiovascular disease, similar to AM, and whether this signaling axis could be therapeutically targeted in lymphatic endothelial cells for the improvement of cardiac repair after injury.

Methods

Ethical approvals

The animal study was reviewed and approved by IACUC 21-083.0.

Molecular cloning

The humanized coding sequences of V5-tagged TurboID[24] (V5-TurboID-NES_pCDNA3; Addgene plasmid #107169) and V5-tagged miniTurbo ID[24] (V5-miniTurbo-NES_pCDNA3; Addgene plasmid #107170) were a gift from Alice Ting. The humanized coding sequence of VE-cadherin (mVenus-VE-Cadherin-N-10; Addgene plasmid #56340) was a gift from Michael Davidson. Entry vectors containing these

Fig. 7 | Lymphatic secretion of reelin requires VE-cadherin plasma membrane junctional organization in vitro and VE-cadherin expression in vivo. A Time course of reelin levels (ng/mL) in conditioned media collected from LECs treated with +/− 100 nM AM and quantified by ELISA. $n = 3$-8 biological replicates (mean ± s.d). Significance was determined using a Mixed-effects model (REML) with Šídák's multiple comparisons test. To examine the effect of VE-cadherin membrane levels on reelin levels (ng/mL) in LEC conditioned media, LECs were treated with +/− 100 nM AM as well as pretreated with (**B**) shCDH5 (48 h), (**C**) 10 μM Rasarfin (4 h), (**D**) 100 μM Endosidin-2 (24 h), or (**E**) shEXOC5 (48 h) and quantified by ELISA. $n = 3$-8 biological replicates for each condition (mean ± s.d). Significance was determined using a Mixed-effects model (REML) (panel **B**), a two-way ANOVA with Geisser-Greenhouse correction (**C** and **E**), or a one-way ANOVA (panel **D**) with Tukey's multiple comparisons test. Statistics only shown for comparisons between samples within a given time point. All comparisons are shown in Supplementary Fig. 10. Shown are representative western blots of plasma membrane fractions from LECs to correlate time-dependent secretion of reelin with changes in plasma membrane levels of VE-cadherin. Actin served as a load control. **F** Serum reelin levels of *Cdh5*$^{\Delta PROX1}$ and littermate *Cdh5*$^{fl/fl}$ (WT) mice before tamoxifen treatment at 1–2 months old (D1, hollow symbols) and 3 weeks after tamoxifen treatment (D22, solid symbols). Significance was determined using a two-way ANOVA with Šídák's multiple comparisons test. $n = 8$ mice per group (mean ± s.d). **F** Created with BioRender.com released under a Creative Commons Attribution-NonCommercial-NoDerivs 4.0 International license. Precise n numbers and p-values are found for each condition in Supplementary Data 10. Source data are provided with this paper.*$p < 0.05$, **$p < 0.01$, ***$p < 0.001$, ****$p < 0.0001$.

humanized coding sequences were cloned into either a pDONR234 or pDONR223 (gifted from the Frederick National Laboratory for Cancer Research) vector using the Gateway™ BP Clonase™ Enzyme mix (ThermoFisher Scientific # 11789100). These entry clones were then utilized to generate p667-Ve-cadherin-V5-TurboID (VE-cadherin-T) and p667-Ve-cadherin-V5-MiniTurboID (VE-cadherin-mT) lentiviral expression clones using the following reagents and destination vectors: Gateway™ LR Clonase™ Enzyme mix (ThermoFisher Scientific # 11791020), C413-E33 (attB4-UbCp > -attB1r) (Addgene plasmid #162925), and pDest-667 (attR4-attR3) (Addgene plasmid #161886). Successful generation of constructs was confirmed via restriction digest, sequencing, and protein expression.

Cell culture

Human embryonic kidney 293 T (HEK293T) cells were maintained in Dulbecco's modified Eagle's medium (DMEM) (Gibco) supplemented with 10% (v/v) fetal bovine serum (Sigma Aldrich), and 1% (v/v) penicillin-streptomycin (Gibco # 15070063) at 37 °C under 5% CO_2. Transient transfection of HEK293T was accomplished via calcium phosphate precipitation. HEK293T cells stably expressing either VE-cadherin-T or VE-cadherin-mT were generated using 100 μL unconcentrated virus + 10 μg/mL polybrene (EMD Milipore, #TR-1003-G) to enhance transduction efficiency and selected using 2 μg/mL puromycin. Primary human dermal lymphatic endothelial cells (LECs) (PromoCell, #C-12216) were cultured in Endothelial Cell Growth Medium (EGM-MV2) bullet kit medium (PromoCell, #C-22121) 37°C under 5% CO_2. LECs were used within 5 passages to avoid differentiation. The following ligands and inhibitors were utilized throughout this study: human Adrenomedullin (Bachem, #4030215.1000), Rasarfin (MedChemExpress, #HY139950), Endosidin2 (Sigma-Aldrich, #SML1681), and (R)-MG132 (Sigma-Aldrich, #M8699).

Lentivirus-mediated expression of (mini)TurboID constructs and shRNA knockdown constructs

Lentiviral particles containing VE-cadherin-T and VE-cadherin-mT were generated in HEK293T cells by the UNC Lenti-shRNA Core Facility. Lentiviral particles containing shRNA targeting of VE-cadherin (pLV[shRNA]-EGFP-CDH5-shRNA1 to be referred to as shCDH5), EXOC5 (TRCN0000061964, TRCN0000061965, TRCN0000061966, TRCN0000061967), human beta globin (HBG) (TRCN0000029094) control (negative control), or a scramble control shRNA (shScramble) (negative control) were generated in HEK293T cells by the UNC Lenti-shRNA Core Facility. Each batch of virus was independently tested for adequate protein expression or knockdown. shEXOC5 and shHGB plasmids were obtained from the UNC Lenti-shRNA Core Facility. Scramble shRNA was a gift from David Sabatini (Addgene plasmid #186453). shCDH5 was a gift from Joshua Scallan[4] and its efficiency was previously validated in prior studies conducted by authors of this study[5]. Transduction was achieved by supplementing HEK293Ts or LECs with media containing 20% v/v unconcentrated viral particles and 10 μg/mL polybrene for 24 h. After 24 h, the media was replaced with fresh growth media and cells were grown for an additional 48 h before performance of experiments.

Plasma membrane isolation

Plasma membrane isolation was performed as previously described and as routinely done to enrich post-synaptic densities[58,59]. Briefly, after appropriate treatment, the LEC media was aspirated, cells were washed with ice cold 1x PBS, and ice cold 1x PBS was added to scrape cells into a 1.7 mL conical tube. While on ice, cells were homogenized by passing 10 times through an insulin syringe (29G1/2). After, homogenized cells were spun at 1000 G for 10 min at 4 °C. The supernatant was collected and transferred to a fresh 1.7 mL tube and then spun at 14,000 G for 20 min at 4 °C. The supernatant was aspirated, and the remaining pellet, which is comprised of the membrane fraction, was either stored at −80 °C or immediately lysed in lysis buffer and rotated for 30 min at 4 °C before protein normalization.

Western blot analysis

Western blot antibodies. The following antibodies and dilutions were used for western analysis: anti-VE Cadherin rabbit polyclonal (Abcam #ab33168) (1:2,000 dilution), anti-β-catenin mouse monoclonal (BD Biosciences #610153) (1:2,000 dilution), anti-actin mouse monoclonal (Sigma-Aldrich #A4700) (1:10,000 dilution), anti-GAPDH mouse monoclonal (Novus Biologicals #NB300-221) (1:10,000 dilution), anti-V5 mouse monoclonal (ThermoFisher Scientific #R960-25) (1:2,000 dilution), anti-afadin rabbit monoclonal (D1Y3Z) (Cell Signaling Technology #13531S) (1:2,000 dilution), anti-EXOC5 rabbit polyclonal (Novus Biologicals #NBP2-31841) (1:2,000 dilution), IRDye® 680 LT Streptavidin (Licor #926-68031) (1:2500 dilution), goat anti-rabbit IR Dye 800 CW (Licor #926-32211) (1:10,000 dilution), goat anti-mouse IR Dye 800 CW (Licor #926-32210) (1:10,000 dilution), goat anti-mouse IR Dye 680 CW (Licor #926-68020) (1:10,000 dilution).

Protein lysis and normalization. The lysis buffer used throughout this study was comprised of 50 mM Tris-HCL (pH 7.4), 150 mM NaCl, 1% NP-40, 0.25% deoxycholate, 1 mM EDTA, 2 M Urea supplemented with protease (cOmpleteTM, EDTA-free Protease Inhibitor Cocktail; ROCHE, #11873580001) and phosphatase (PhosSTOP EASYpack; ROCHE, #4906845001) inhibitors as well as Benzonase® nuclease (Millipore, #E1014). Protein levels in cell lysates were determined by Pierce™ BCA protein assay (ThermoFisher Scientific, #23225) and normalized to allow for comparisons between conditions.

Streptavidin affinity-purification and western blotting. For streptavidin affinity-purification followed by western blot analysis, 30 μL per a sample of streptavidin Sepharose high performance bead slurry (GE Healthcare #17-5113-01) was added to normalized cell lysates and samples were rotated for 24 h at 4 °C. After, beads were washed 5 times in lysis buffer and protein was eluted off beads through addition of a 1:1:1 mixture of 4x LDS buffer (Invitrogen #NP0007): Lysis buffer: 1 M DTT and boiled for 10 min at 95 °C.

Normalized cell lysates and/or streptavidin-affinity purified biotinylated proteins were separated on a 4–12% NuPAGE™ Bis Tris gel (ThermoFisher Scientific, #NPO335BOX or NP0336BOX) using 1x MOPS-SDS Running Buffer (Boston BioProducts, #BP-178), transferred to a nitrocellulose membrane using 2x Bis-Tris Transfer Buffer (Boston BioProducts, #BP-193) supplemented with 20% methanol, and imaged on a Licor Odyssey CLx using Image Studio Ver 5.2. Densitometry was done using ImageJ software (version 1.52a) and graphs represent the ratio of protein (VE-cadherin or β-catenin) to load control and normalized to control sample for comparison between independent experiments.

Validation of TurboID and miniTurboID Constructs. HEK293T cells transiently and stably expressing the newly generated VE-cadherin-T and VE-cadherin-mT expression clones were utilized for construct validation and assay optimization. Briefly, 2×10^6 HEK293T cells were seeded into a 10 cm plate. Once cells were confluent, 50 μM biotin was added to cells for appropriate length of time. After, the media was immediately replaced with ice-cold 1x PBS to stop further biotinylation and cells were washed in ice-cold 1x PBS, lysed, and normalized. Western blot analysis was performed on input and streptavidin-AP biotinylated proteins to determine construct expression and biotinylation.

To Examine VE-cadherin Total and Plasma Membrane Protein Levels. LECs were seeded at 1.0×10^6 cells per 10 cm plate for plasma membrane isolation and at 1.5×10^5 cells per well of 6-well plate for total protein expression and grown for 24 h. To determine the effect of gene knockdown on VE-cadherin plasma membrane or total levels, cells were infected the following day with either shScramble, shCDH5, or shEXOC5 (450 μL unconcentrated virus supplemented with 10 μg/mL polybrene per 10-cm plate). The following day, media was replaced with fresh growth media and cells were allowed to grow for an additional 48 h prior to AM treatment and protein isolation. To determine the effect of exocyst inhibitors (100 μM Endosidin-2 or 10 μM Rasarfin) on VE-cadherin plasma membrane or total levels, cells were grown to near confluency, after which, were treated with either inhibitor or vehicle (DMSO) +/− 100 nM AM for appropriate time. For both shRNA and inhibitor experiments, cellular signaling was arrested through addition of ice-cold 1x PBS followed by plasma membrane isolation (see *Plasma Membrane Isolation* section above), if appropriate, and cellular lysis. Protein levels were normalized, and western blot analysis was performed.

Capture of biotinylated VE-cadherin proximal proteins

Sample preparation. The proximity protein interactome of VE-cadherin was identified in LECs using the following protocols. Expression of VE-cadherin-mT fusion protein within LECs was achieved through transduction of LECs with lentivirus containing VE-cadherin-mT and supplemented with 10 μg/mL polybrene. After 24 h, media was changed to fresh endothelial cell growth media and cells were allowed to proliferate for an additional 48 h before media was supplemented with 50 μM biotin and +/− 100 nM AM for 2 h. After a 2 h labeling period, signaling and biotinylation was quenched by aspirating the biotin-enriched media and washing cells with ice-cold 1x PBS.

Enrichment of biotinylated proteins by streptavidin affinity purification. For streptavidin affinity-purification followed by LC-MS/MS, 100 μL/ sample of Dynabeads MyOne Steptavidin T1 (ThermoFisher, #65601) slurry was utilized (GE Healthcare, #17-5113-01) per 2.5 mg of whole cell lysate or 50–100 ug of membrane fractions. Upon addition of washed beads, samples were rotated for 24 h at 4 °C. After, beads were washed 4 times in lysis buffer followed by an additional 4 washes in ammonium bicarbonate buffer (ABC) (50 mM, pH 7.8). After final wash, beads were resuspended in 50 μL ABC buffer (pH 7.8) and stored at −80 °C until submission to the UNC Michael Hooker Proteomics Center for on-bead trypsin digestion and LC-MS/MS analysis.

LC-MS/MS

Three independent LC-MS/MS experiments (Supplementary Data 1, 2, and 6) were performed on streptavidin-affinity purified biotinylated proteins enriched from LECs transduced with lentivirus for expression of VE-cadherin-mT. Experimental details including replicate numbers and analysis performed can be found in Supplementary Table 1. Biotinylated proteins captured on streptavidin-coated magnetic beads (Dynabeads MyOne Streptavidin T1, ThermoFisher, 65601) were subject to on-bead trypsinization (1 μg trypsin; Promega), acidified to 2% formic acid, and subsequent C18 desalting cleaning. Samples were injected onto an Easy Spray PepMap C18 column (75μm id 588 × 25 cm, 2μm particle size) (Thermo Scientific). Samples were analyzed by LC-MS/MS using an Easy nLC 1200 coupled to a QExactive 587 HF (Thermo Scientific). Liquid chromatography and HCD fragmentation were done by the Hooker Proteomics Center as previously described[60]. The mass spectrometry proteomics data have been deposited to the ProteomeXchange Consortium (http://www.proteomexchange.org/) via the PRIDE[61] partner repository (https://www.ebi.ac.uk/pride/) with the dataset identifier PXD040452.

Proteomic data analysis

Raw data were processed using MaxQuant (v1.6.15.0) for identification and label-free quantification (LFQ) and searched against the Uniprot Reviewed protein database for human proteins (downloaded October 2020, containing ~20,381 entries) and an appended common contaminants database (~250 sequences) using Andromeda within MaxQuant. The maximum allowed missed tryptic cleavage sites was set to 2 and variable modifications specified were methionine oxidation and N-terminus acetylation. A 1% FDR threshold was set and match between runs was enabled. MS/MS mass tolerance was set to 20 ppm. Label free quantification using LFQ intensities required a minimum of two unique peptides. The Perseus (version 1.6.14.0) software platform was used to filter and analyze MaxQuant results. Common mass spectrometry contaminants, reverse hits, and proteins with one peptide identified or 50% missing values were removed. Imputation of missing values was performed from a normal distribution. Averaged Log2 LFQ intensities of sample relative to control were calculated; 'biotin' versus 'biotin + AM' for whole cell lysate samples and 'biotin only' or 'biotin + AM' versus 'no biotin control' for plasma membrane samples. The analysis results are reported in Supplementary Data 1, 2, and 6. Statistical analysis utilized a paired, two-tailed students *t*-test between samples.

Bioinformatic analyses

Pathway analyses. Gene Ontology (GO) terms for individual proteins were obtained from IPA analyses and the Uniprot database, and these terms were subsequently used for manual curation of the mass spectrometry datasets. ShinyGO (Version 0.76.3) was used to perform GO analysis for cellular component, biological process, and molecular function[29–31]. Reactome pathway knowledgebase[32] (version 78) was used to identify pathways represented in all proteins identified within the plasma membrane data set. The cell-cell junction organization pathway (Released 9-30-2009, https://doi.org/10.3180/REACT_23419.1; Stable Identifier R-HSA-421270) was examined for overlap with proteins reliably identified in the VE-cadherin interactome. QIAGEN Ingenuity Pathway Analysis (IPA) (version 70750971; release date 2021-10-22) was utilized to identify canonical pathways and relationships of proteins identified in the VE-cadherin interactome and to determine the effect of AM-mediated reorganization on these pathways. IPA performed on WCL1 utilizing log2 fold change of each protein upon AM treatment (AM vs. No AM). IPA performed on PM utilized log2 fold

change of each protein for each listed condition (Biotin vs. No Biotin, Biotin + AM vs No Biotin, and Biotin + AM vs. Biotin).

Interactome comparison analyses. BioID- identified interactomes for E-cadherin and N-cadherin were obtained from previously published reports (Guo et al.[19] and Li et al.[21],also found in Supplementary Data 5). BioVenn[33] software was used to generate a Venn diagram comparing the E-cadherin, N-cadherin, and VE-cadherin interactomes. The cellular functions of proteins identified in all three interactomes were classified according to functional categories aggregated from Uniprot, GeneCards and Entrez, in similar fashion to categorizations done by the authors of the N-cadherin interactome study[21]. In addition, BioVenn was used to compare the whole cell (WCL1) and plasma membrane (PM) VE-cadherin interactomes.

Immunofluorescence staining and microscopy

Immunofluorescence staining and microscopy was performed by seeding 1.2×10^5 HEK293Ts or LECs onto 35 mm poly-D-lysine coated culture plates with a 10 mm diameter glass coverslip bottom (MatTek # P35GC-0-10-C). To test biotinylation efficiency and localization of VE-cadherin-mT, cells were transduced with VE-cadherin-mT lentivirus (20% v/v virus, with 10 μg/mL polybrene) as previously described and the media was supplemented with 50 μM biotin and +/− 100 nM AM or vehicle for designated time-points.

To test the effect of EXOC5 gene knockdown (shEXOC5) on VE-cadherin localization, LECs were transduced with shScramble or shEXOC5 (20% v/v virus, with 10 μg/ mL polybrene) for 24 h, followed by a media change and 48 h growth period before treatment with 100 nM AM or vehicle for 4 h. To test the effect of Endosidin-2 on VE-cadherin localization, cells were treated with 100 μM Endosidin-2 (Sigma-Aldrich, #SML1681) or vehicle (DMSO) for 24 h followed by 4 h treatment with 100 nM AM. To test the effect of Rasarfin on VE-cadherin localization, VE-cadherin-mT transduced LECs were co-treated with 10 μM Rasarfin (MedChem Express, #HY-139950) and 100 nM AM or vehicle (DMSO) for 4 h.

After appropriate treatments, HEK293T or LECs were fixed in 4% PFA for 30 min followed by 3 × 5 min washes using 1x PBS. Cells were then permeabilized using 0.2% Triton X-100 for 2 min, followed by another round of 3 × 5 minute washes using 1x PBS. After, cells were blocked with 4% BSA or 5% Normal Donkey Serum (Jackson ImmunoResearch, #017-000-121) in 1x PBS for 1 h at room temperature prior to addition of rabbit anti-VE-cadherin IgG (1:200 dilution; Abcam, #ab33168) for 24 h at 4 °C. The next day, the cells were washed 3X for 5 min with 1x PBS prior to addition of the appropriate secondary antibodies for 2 h at room temperature: AffiniPure Donkey anti-mouse IgG Cy3 (1:200, Jackson ImmunoResearch, #715-165-150), AffiniPure Donkey anti-Rabbit IgG Cy5 (1:100, Jackson ImmunoResearch, #711-175-152), or Streptavidin AlexaFluor 488 (1:200, Invitrogen, #S11223). After, the cells were washed 3X for 5 min with 1x PBS and nuclei were stained with Bisbenzimide H 33258 (Hoechst, 1:1000, Sigma-Aldrich, #B1155). Cells were imaged on either a Zeiss 880 confocal laser scanning microscope (ZEN software version 2.3 SP1) or an Olympus IX83 microscope with a Hamamatsu Orca Flash 4.0 camera using CellSen Dimension software (version 1.18). Images were processed in FIJI[62] (version 1.54b) to pseudo color channels, scale bars were added, and brightness was uniformly adjusted. Representative images which depict the median phenotype/response for each treatment and experiment were chosen for inclusion in the manuscript.

qPCR

To evaluate shCDH5 or shEXOC5 knockdown efficiency (VE-cadherin or EXOC5, respectively) as well as determine the effect of shEXOC5 or inhibitor treatment (Rasarfin or Endosidin-2) on VE-cadherin transcript levels, LECs were seeded at 2.0×10^5 cells/well into 6-well plates in EGM-MV2 endothelial growth media. First, to evaluate VE-cadherin or EXOC5 knockdown efficiency, LECs were transduced with control lentivirus (either shScramble or shHGB), shCDH5, or one of four shEXOC5 clones as previously described. To evaluate the effect of shEXO5, Rasarfin, or Endosidin-2 treatment on VE-cadherin mRNA transcript levels, LECs were transduced with shEXOC5 as previously described or treated simultaneously with 100 nM AM + /− 10 μM Rasarfin or 100 μM Endosidin-2 for 4- and 24 h prior to mRNA isolation.

After appropriate treatments, LECs were washed with 1x PBS, lysed in TRIzol Reagent (Invitrogen, Thermo Fisher Scientific, #15596026), and isolated mRNA was reverse transcribed using M-MLV reverse transcriptase (ThermoFisher Scientific, #28025013). Quantitative gene expression was assayed with TaqMan Fast Advanced Master Mix (Applied Biosystems, #4444554) and run on a StepOnePlus Real-Time PCR System with StepOne software v2.3 (Applied Biosystems) set for a fast 96-well (0.1 mL) block. The reaction volume per well was 20 μL. The following thermocycle protocol was utilized: (1) A hold stage from 25 °C to 95 °C at a rate of 2.63 °C/sec. Hold at 95 °C for 20 s (00:20) then (2) PCR stage−Step 1: 2.63 °C/s to 95 °C for 1 s (00:01); Step 2−from 95 °C to 60 °C at a rate of 2.42 °C/s, and hold at 60 °C for 20 s (00:20). PCR was set for 40 cycles. The following ThermoFisher Taqman gene expression assay probes were used: *CDH5*- HS00901465_m1, *EXOC5*- HS00272473_m1 and *ACTB*-HS01060665_g1. ΔΔCt values normalized to either wild type or control (shHGB or shScramble) cells are shown (housekeeping gene: *ACTB*).

Reelin ELISA on LEC conditioned media

LECs were seeded at 1.2×10^5 cells/well in 6-well plates in EGM-MV2 endothelial growth media. Prior to collection of reelin conditioned media, cells were serum starved overnight in Opti-MEM (Gibco, #31985070) and then media was replaced with 1.5 mL of Opti-MEM supplemented with and without 100 nM AM. Conditioned media was collected at appropriate time-points and reelin levels were assayed in the undiluted conditioned media using a commercially available colorimetric human Reelin ELISA kit (Abcam, #ab284620) and read on a Biotek Cytation5 plate reader using Gen5 software (version 3.11).

For conditions testing the effect of gene knockdown, cells were transduced with either shScramble, shCDH5, or shEXOC5 lentivirus as previously described. For conditions testing Endosidin-2 treatment, either vehicle (DMSO) or 100 μM Endosidin-2 was added to the Opti-MEM media during overnight serum starvation. For conditions testing Rasarfin treatment, either vehicle (DMSO) or 10 μM Rasarfin was added simultaneous to AM treatment.

Reelin ELISA on *Cdh5*$^{fl/fl}$; *Prox1*^{CreERT2} mice

Cdh5$^{fl/fl}$ mice were a gift from Dr. Dietmar Vestweber[63]. *Prox1*^{CreERT2} mice were a gift from Dr. Taija Mäkinen[64]. VE-cadherin deletion was induced in 1–2 months old *Cdh5*$^{fl/fl}$; *Prox1*^{CreERT2} and littermate *Cdh5*$^{fl/fl}$ mice using intraperitoneal injection of 50 μg Tamoxifen (Sigma-Aldrich, #T5648, dissolved in corn oil) per gram of bodyweight on days 1,2, 3, 5, and 8, as reported previously[5]. To measure serum reelin levels, serum was collected from male and female mice before Tamoxifen treatment at 1–2 months old, and 3 weeks after Tamoxifen treatment. Whole blood was obtained by retro-orbital bleed. The samples were allowed to coagulate for 30 min on ice and then centrifuged for 10 min at 2300 G. The serum was saved at −80 °C until used for analysis. Reelin levels were determined using reelin-specific ELISA kit (Abcam, #ab284620). All animal studies were approved by the Institutional Animal Care and Use Committee of UNC-Chapel Hill (IACUC protocol #21-083.0). Animal housing (12 h light/dark cycle, at 18–23 degrees Celsius and 40–60% humidity), care, and husbandry were overseen by the UNC Division of Comparative Medicine Animal Resources, which is accredited by the Association for Assessment and Accreditation of Laboratory Animal Care (AAALAC).

Study design and statistical analyses

Sample size was determined based on a priori experience or based on published literature utilizing similar assays, in accordance with best practices in the field. Data was collected and analyzed without bias whenever possible. Blinding was used by investigators performing the during the processing, running and analysis of the mass spectrometry. Image analyses were performed blinded. Unless otherwise noted, statistical analyses were performed using GraphPad Prism version 10. All data are presented as mean ± SD. Normality of distribution was assessed using the Shapiro-Wilk test. Student two-tailed unpaired *t*-test was used to analyze the differences between 2 groups when appropriate. One-way ANOVA with Tukey's or Dunnett's multiple comparisons was used when appropriate. Mixed-effects model (REML) with Šídák's or Tukey's multiple comparisons test was used to determine equality testing between three or more means. Two-way ANOVA with Geisser-Greenhouse correction with Tukey's multiple comparisons was used to determine the interrelationship of two or more independent variables on a dependent variable (i.e. treatment and time). Significance for all tests was considered when $P < 0.05$. A detailed description of precise n numbers, normality testing, statistical tests utilized, comparisons made, and exact *p*-values are included in Supplementary Data 10.

Reporting summary

Further information on research design is available in the Nature Portfolio Reporting Summary linked to this article.

Data availability

The mass spectrometry proteomics data have been deposited to the ProteomeXchange Consortium (http://www.proteomexchange.org/) via the PRIDE[61] partner repository (https://www.ebi.ac.uk/pride/) with the dataset identifier PXD040452. Additionally. Source data are provided with this paper.

References

1. Gulino, D. et al. Alteration of endothelial cell monolayer integrity triggers resynthesis of vascular endothelium cadherin. *J. Biol. Chem.* **273**, 29786–29793 (1998).
2. Matsuyoshi, N. et al. In vivo evidence of the critical role of cadherin-5 in murine vascular integrity. *Proc. Assoc. Am. Physicians* **109**, 362–371 (1997).
3. Hägerling, R. et al. Distinct roles of VE-cadherin for development and maintenance of specific lymph vessel beds. *EMBO J.* **37**, e98271 (2018).
4. Yang, Y., Cha, B., Motawe, Z. Y., Srinivasan, R. S. & Scallan, J. P. VE-cadherin is required for lymphatic valve formation and maintenance. *Cell Rep.* **28**, 2397–2412.e4 (2019).
5. Harris, N. R. et al. VE-cadherin is required for cardiac lymphatic maintenance and signaling. *Circ. Res.* **130**, 5–23 (2022).
6. Baluk, P. et al. Functionally specialized junctions between endothelial cells of lymphatic vessels. *J. Exp. Med.* **204**, 2349–2362 (2007).
7. Dejana, E., Orsenigo, F., Molendini, C., Baluk, P. & McDonald, D. M. Organization and signaling of endothelial cell-to-cell junctions in various regions of the blood and lymphatic vascular trees. *Cell Tissue Res.* **335**, 17–25 (2009).
8. Delva, E. & Kowalczyk, A. P. Regulation of cadherin trafficking. *Traffic* **10**, 259–267 (2009).
9. Giannotta, M., Trani, M. & Dejana, E. VE-cadherin and endothelial adherens junctions: active guardians of vascular integrity. *Dev. Cell.* **26**, 441–454 (2013).
10. Vestweber, D., Winderlich, M., Cagna, G. & Nottebaum, A. F. Cell adhesion dynamics at endothelial junctions: VE-cadherin as a major player. *Trends Cell Biol.* **19**, 8–15 (2009).
11. Vestweber, D. VE-cadherin: the major endothelial adhesion molecule controlling cellular junctions and blood vessel formation. *Arterioscler Thromb. Vasc. Biol.* **28**, 223–232 (2008).
12. Pflicke, H. & Sixt, M. Preformed portals facilitate dendritic cell entry into afferent lymphatic vessels. *J. Exp. Med.* **206**, 2925–2935 (2009).
13. Dunworth, W. P., Fritz-Six, K. L. & Caron, K. M. Adrenomedullin stabilizes the lymphatic endothelial barrier in vitro and in vivo. *Peptides* **29**, 2243–2249 (2008).
14. Yao, L. C., Baluk, P., Srinivasan, R. S., Oliver, G. & McDonald, D. M. Plasticity of button-like junctions in the endothelium of airway lymphatics in development and inflammation. *Am. J. Pathol.* **180**, 2561–2575 (2012).
15. Zheng, W. et al. Angiopoietin 2 regulates the transformation and integrity of lymphatic endothelial cell junctions. *Genes Dev.* **28**, 1592–1603 (2014).
16. Xu, W. et al. Small GTPase Rap1A/B is required for lymphatic development and adrenomedullin-induced stabilization of lymphatic endothelial junctions. *Arterioscler Thromb. Vasc. Biol.* **38**, 2410–2422 (2018).
17. Roux, K. J., Kim, D. I., Raida, M. & Burke, B. A promiscuous biotin ligase fusion protein identifies proximal and interacting proteins in mammalian cells. *J. Cell Biol.* **196**, 801–810 (2012).
18. Van Itallie, C. M. et al. The N and C termini of ZO-1 are surrounded by distinct proteins and functional protein networks. *J. Biol. Chem.* **288**, 13775–13788 (2013).
19. Guo, Z. et al. E-cadherin interactome complexity and robustness resolved by quantitative proteomics. *Sci. Signal.* **7**, rs7 (2014).
20. Van Itallie, C. M. et al.Biotin ligase tagging identifies proteins proximal to E-cadherin, including lipoma preferred partner, a regulator of epithelial cell-cell and cell-substrate adhesion. *J. Cell Sci.* **127**, 885–895 (2014).
21. Li, Y. et al. The N-cadherin interactome in primary cardiomyocytes as defined using quantitative proximity proteomics. *J. Cell Sci.* **132**, jcs221606 (2019).
22. Fredriksson, K. et al. Proteomic analysis of proteins surrounding occludin and claudin-4 reveals their proximity to signaling and trafficking networks. *PLoS One* **10**, e0117074 (2015).
23. Sears, R. M., May, D. G. & Roux, K. J. BioID as a tool for protein-proximity labeling in living cells. *Methods Mol. Biol.* **2012**, 299–313 (2019).
24. Branon, T. C. et al. Efficient proximity labeling in living cells and organisms with TurboID. *Nat. Biotechnol.* **36**, 880–887 (2018).
25. Baluk, P. & McDonald, D. M. Buttons and zippers: endothelial junctions in lymphatic vessels. *Cold Spring Harb. Perspect. Med.* **12**, a041178 (2022).
26. Breslin, J. W. et al. Lymphatic vessel network structure and physiology. *Compr. Physiol.* **9**, 207–299 (2018).
27. Kim, D. I. et al. Probing nuclear pore complex architecture with proximity-dependent biotinylation. *Proc. Natl Acad. Sci. USA* **111**, E2453–E2461 (2014).
28. May, D. G., Scott, K. L., Campos, A. R. & Roux, K. J. Comparative application of BioID and TurboID for protein-proximity biotinylation. *Cells* **9**, 1070 (2020).
29. Ge, S. X., Jung, D. & Yao, R. ShinyGO: a graphical gene-set enrichment tool for animals and plants. *Bioinformatics* **36**, 2628–2629 (2020).
30. Kanehisa, M., Furumichi, M., Sato, Y., Ishiguro-Watanabe, M. & Tanabe, M. KEGG: integrating viruses and cellular organisms. *Nucleic Acids Res.* **49**, D545–D551 (2021).
31. Luo, W. & Brouwer, C. Pathview: An R/bioconductor package for pathway-based data integration and visualization. *Bioinformatics* **29**, 1830–1831 (2013).
32. Segev, N. GTPases in intracellular trafficking: an overview. *Semin Cell Dev. Biol.* **22**, 1–2 (2011).

33. Hulsen, T., de Vlieg, J. & Alkema, W. BioVenn—a web application for the comparison and visualization of biological lists using area-proportional Venn diagrams. *BMC Genom.* **9**, 488 (2008).
34. Wheeler, M. A., Warley, A., Roberts, R. G., Ehler, E. & Ellis, J. A. Identification of an emerin-beta-catenin complex in the heart important for intercalated disc architecture and beta-catenin localisation. *Cell Mol. Life Sci.* **67**, 781–796 (2010).
35. Gillespie, M. et al. The reactome pathway knowledgebase 2022. *Nucleic Acids Res.* **50**, D687–d692 (2022).
36. Palacios, F., Price, L., Schweitzer, J., Collard, J. G., & D'souza-schorey, C. An essential role for ARF6-regulated membrane traffic in adherens junction turnover and epithelial cell migration. *EMBO J.* **20**, 4973–4986 (2001).
37. Moskalenko, S. et al. The exocyst is a Ral effector complex. *Nat. Cell Biol.* **4**, 66–72 (2002).
38. Wirtz-Peitz, F. & Zallen, J. A. Junctional trafficking and epithelial morphogenesis. *Curr. Opin. Genet Dev.* **19**, 350–356 (2009).
39. Prigent, M. et al. ARF6 controls post-endocytic recycling through its downstream exocyst complex effector. *J. Cell Biol.* **163**, 1111–1121 (2003).
40. Samak, G. et al. Cyclic stretch disrupts apical junctional complexes in caco-2 cell monolayers by a JNK-2-, c-Src-, and MLCK-dependent mechanism. *Am. J. Physiol. Gastrointest. Liver Physiol.* **306**, G947–G958 (2014).
41. D'Arcangelo, G. Reelin in the years: controlling neuronal migration and maturation in the mammalian brain. *Adv. Neurosci.* **2014**, 597395 (2014).
42. Lutter, S., Xie, S., Tatin, F. & Makinen, T. Smooth muscle-endothelial cell communication activates Reelin signaling and regulates lymphatic vessel formation. *J. Cell Biol.* **197**, 837–849 (2012).
43. Liu, X. et al. Lymphoangiocrine signals promote cardiac growth and repair. *Nature* **588**, 705–711 (2020).
44. Bryan, B. A. & D'Amore, P. A. What tangled webs they weave: Rho-GTPase control of angiogenesis. *Cell Mol. Life Sci.* **64**, 2053–2065 (2007).
45. Van Acker, T., Tavernier, J. & Peelman, F. The small GTPase Arf6: an overview of its mechanisms of action and of its role in host(-) pathogen interactions and innate immunity. *Int J. Mol. Sci.* **20**, 2209 (2019).
46. Lundberg, O. H. M. et al. Bioactive adrenomedullin in sepsis patients in the emergency department is associated with mortality, organ failure and admission to intensive care. *PLoS One* **17**, e0267497 (2022).
47. Valenzuela-Sánchez, F., Valenzuela-Méndez, B., Rodríguez-Gutiérrez, J. F., Estella-García, Á. & González-García, M. New role of biomarkers: mid-regional pro-adrenomedullin, the biomarker of organ failure. *Ann. Transl. Med.* **4**, 329 (2016).
48. Nuki, C. et al. Vasodilator effect of adrenomedullin and calcitonin gene-related peptide receptors in rat mesenteric vascular beds. *Biochem Biophys. Res Commun.* **196**, 245–251 (1993).
49. Di Iorio, R. et al. Adrenomedullin, a new vasoactive peptide, is increased in preeclampsia. *Hypertension* **32**, 758–763 (1998).
50. Harris, N. R. et al. The ebb and flow of cardiac lymphatics: a tidal wave of new discoveries. *Physiol. Rev.* **103**, 391–432 (2023).
51. Klein, K. R. & Caron, K. M. Adrenomedullin in lymphangiogenesis: from development to disease. *Cell Mol. Life Sci.* **72**, 3115–3126 (2015).
52. Wong, H. K., Cheung, T. T. & Cheung, B. M. Adrenomedullin and cardiovascular diseases. *JRSM Cardiovasc. Dis.* **1**, 1–7 (2012).
53. Trincot, C. E. et al. Adrenomedullin induces cardiac lymphangiogenesis after myocardial infarction and regulates cardiac edema via connexin 43. *Circ. Res.* **124**, 101–113 (2019).
54. Caron, K. M. & Smithies, O. Extreme hydrops fetalis and cardiovascular abnormalities in mice lacking a functional adrenomedullin gene. *Proc. Natl Acad. Sci. USA* **98**, 615–619 (2001).
55. Dackor, R. T. et al. Hydrops fetalis, cardiovascular defects, and embryonic lethality in mice lacking the calcitonin receptor-like receptor gene. *Mol. Cell Biol.* **26**, 2511–2518 (2006).
56. Wetzel-Strong, S. E., Li, M., Klein, K. R., Nishikimi, T. & Caron, K. M. Epicardial-derived adrenomedullin drives cardiac hyperplasia during embryogenesis. *Dev. Dyn.* **243**, 243–256 (2014).
57. Klein, K. R. et al. Decoy receptor CXCR7 modulates adrenomedullin-mediated cardiac and lymphatic vascular development. *Dev. Cell.* **30**, 528–540 (2014).
58. Chiu, S. L. et al. GRASP1 regulates synaptic plasticity and learning through endosomal recycling of AMPA receptors. *Neuron* **93**, 1405–1419.e8 (2017).
59. Rajkumar, S., Bockers, T. M. & Catanese, A. Fast and efficient synaptosome isolation and post-synaptic density enrichment from hiPSC-motor neurons by biochemical sub-cellular fractionation. *STAR Protoc.* **4**, 102061 (2023).
60. Gerlach, G. F., Imseis, Z. H., Cooper, S. L., Santos, A. N. & O'Brien, L. L. Mapping of the podocin proximity-dependent proteome reveals novel components of the kidney podocyte foot process. *Front Cell Dev. Biol.* **11**, 1195037 (2023).
61. Perez-Riverol, Y. et al. The PRIDE database resources in 2022: a hub for mass spectrometry-based proteomics evidences. *Nucleic Acids Res.* **50**, D543–D552 (2022).
62. Schindelin, J. et al. Fiji: an open-source platform for biological-image analysis. *Nat. Methods* **9**, 676–682 (2012).
63. Frye, M. et al. Interfering with VE-PTP stabilizes endothelial junctions in vivo via tie-2 in the absence of VE-cadherin. *J. Exp. Med.* **212**, 2267–2287 (2015).
64. Bazigou, E. et al. Integrin-alpha9 is required for fibronectin matrix assembly during lymphatic valve morphogenesis. *Dev. Cell* **17**, 175–186 (2009).

Acknowledgements

We thank Dr. Benjamin Major and Dr. Dhaval Patel (Washington University in St. Louis, Department of Cell Biology and Physiology) for reagents and assistance in gateway cloning of VE-cadherin-T and VE-cadherin-mT constructs and Dr. Graham Diering (UNC, Department of Cell Biology and Physiology) for providing guidance and protocols for LEC plasma membrane isolation. Further, we thank Dr. Dietmar Vestweber (Max Plank Institute for Molecular Biomedicine, Münster, Germany) for graciously gifting us the *Cdh5*$^{fl/fl}$ mice, Dr. Taija Mäkinen (Uppsala University, Sweden) for graciously gifting us the *Prox1*^{CreERT2} mice, and Dr. Friedemann Keiffer (Max Plank Institute for Molecular Biomedicine, Münster, Germany) for providing expertize on serum collection for performance of the in vivo reelin ELISA. Finally, we thank the UNC Proteomics Core Facility, the UNC Hooker Imaging Core, and the UNC Lenti-shRNA Core Facility for their expertize and services as well as all members of the Caron lab for their constructive and helpful advice throughout this project. This research is based in part upon work conducted using the UNC Proteomics Core Facility and the UNC Hooker Imaging Core, which are both supported in part by P30 CA016086 Cancer Center Core Support Grant to the UNC Lineberger Comprehensive Cancer Center. This work was supported by National Institutes of Health (NIH) grants from the National Heart, Lung, and Blood Institute (NHLBI) HL1290986 and National Institute of Diabetes and Digestive and Kidney Diseases DK119145 and an American Heart Association (AHA) Innovator Award to K.M. Caron, a NHLBI T32HL069768 and an AHA Predoctoral Fellowship no. 834898 to N.R. Harris, a NIH National Cancer Institute T32CA071341 and a NHLBI F31 HL163885 Predoctoral Fellowship to D.S. Serafin, and an AHA Postdoctoral Fellowship 23POST1022945 to L. Bálint.

Author contributions

D.S.S. and N.R.H. designed and performed research studies, analyzed data and generated figures, wrote and edited the manuscript, and acquired independent funding. L.B. and E.S.D. designed and performed the in vivo mouse study, analyzed the data, generated the figure, and edited the manuscript. K.M.C. designed research studies, supervised all aspects of the research, edited the manuscript, and acquired funding.

Competing interests

The authors declare no competing interest.

Additional information

Supplementary information The online version contains supplementary material available at https://doi.org/10.1038/s41467-024-51918-1.

Correspondence and requests for materials should be addressed to Kathleen M. Caron.

Peer review information *Nature Communications* thanks the anonymous reviewers for their contribution to the peer review of this work. A peer review file is available.